Acetylated tau exacerbates learning and memory impairment by disturbing with mitochondrial homeostasis

Qian Liu [a,1], Xin Wang [a,b,1], Yu Hu [c], Jun-Ning Zhao [a], Chun-Hui Huang [d], Ting Li [a], Bing-Ge Zhang [a], Ye He [a], Yan-Qing Wu [e], Zai-Jun Zhang [d,*], Guo-Ping Wang [c,**], Gong-Ping Liu [a,b,***]

[a] *Department of Pathophysiology, School of Basic Medicine, Key Laboratory of Education Ministry of China/Hubei Province for Neurological Disorders, Tongji Medical College, Huazhong University of Science and Technology, Wuhan, 430030, China*
[b] *Co-innovation Center of Neuroregeneration, Nantong University, Nantong, Jiangsu, China*
[c] *Department of Pathology, School of Basic Medicine, Tongji Medical College, Huazhong University of Science and Technology, Wuhan, 430030, China*
[d] *Guangdong Province Key Laboratory of Pharmacodynamic, Constituents of TCM and New Drugs Research, Institute of New Drug Research, College of Pharmacy, Jinan University, Guangzhou, 510632, China*
[e] *Department of Neurology, The Central Hospital of Wuhan, Tongji Medical College, Huazhong University of Science and Technology, Wuhan, 430014, China*

ARTICLE INFO

ABSTRACT

Increased tau acetylation at K274 and K281 has been observed in the brains of Alzheimer's disease (AD) patients and animal models, and mitochondrial dysfunction are noticeable and early features of AD. However, the effect of acetylated tau on mitochondria has been unclear until now. Here, we constructed three type of tau forms, acetylated tau mutant by mutating its K274/K281 into Glutamine (TauKQ) to mimic disease-associated lysine acetylation, the non-acetylation tau mutant by mutating its K274/K281 into Arginine (TauKR) and the wild-type human full-length tau (TauWT). By overexpression of these tau forms in vivo and in vitro, we found that, TauKQ induced more severe cognitive deficits with neuronal loss, dendritic plasticity damage and mitochondrial dysfunctions than TauWT. Unlike TauWT induced mitochondria fusion, TauKQ not only induced mitochondria fission by decreasing mitofusion proteins, but also inhibited mitochondrial biogenesis via reduction of PGC-1a/Nrf1/Tfam levels. TauKR had no significant difference in the cognitive and mitochondrial abnormalities compared with TauWT. Treatment with BGP-15 rescued impaired learning and memory by attenuation of mitochondrial dysfunction, neuronal loss and dendritic complexity damage, which caused by TauKQ. Our data suggested that, acetylation at K274/281 was an important post translational modification site for tau neurotoxicity, and BGP-15 is a potential therapeutic drug for AD.

1. Introduction

Alzheimer's disease (AD) is a neurodegenerative disease characterized by progressive cognitive impairments with an incidence of about 2%–7% among the elderly people over the age of 65, and it is an important cause of dementia in the elderly [1]. Despite the increasing studies on AD, the specific mechanisms of AD onset and development are still unclear, and its therapy is limited to symptomatic treatment, lacking effective prevention and cure. As a cytoskeletal protein, tau protein is significant to the development and function of the nervous system, and its abnormal aggregation is to be one of the main pathological features of AD, while the abnormal post-transcriptional modifications of tau protein is also an important pathological marker for AD [2,3]. Many post-translational modifications of tau exist, the most common being phosphorylation [4–7], others including acetylation [8–11], ubiquitination [12,13], SUMOylation [14], and glycosylation [15,16].

Acetylation of tau is more complex than phosphorylation, and different sites have diametrically opposed effects on tau pathology and cognition. Recently, researchers have found that tau protein can be modified by acetylation at multiple sites. Acetylated tau at the K274 and K281 sites was remarkably increased in the early stages of AD, and more significantly in the brains of advanced AD patients with severe dementia [9, 17]. It has been reported that excessive acetylation of tau at K174 [17], K274 [9], K280 [18], and K281 [9] sites, hinders the degradation of tau and makes tau aggregate more severely. Tau protein can be catalyzed by acetyltransferase p300 and CBP (CREB-binding protein). In AD transgenic mice (PS19), administration of p300 inhibitor salsalate (SSA) reduced acetylated and total tau protein, and attenuated the memory impairment of AD mice [17]. These results suggest that acetylation of tau protein plays an important role in the occurrence and development of AD, and is involved in regulating pathological changes including tau protein phosphorylation and cognitive dysfunction.

In the central nervous system (CNS), adequate energy supply for neuronal survival and activity is largely dependent on mitochondrial sources, therefore, the brain is more vulnerable to mitochondrial dysfunction [19]. Mitochondrial fusion and fission are mainly regulated by two different groups of proteins. The fusion proteins mainly include mitofusin 1/2 (Mfn1/2), optic atrophy-1 protein (Opa1), while mitochondrial fission is regulated by dynamin-related protein (Drp1) and mitochondrial fission 1 protein (Fis1) [20]. Decreased mitochondrial biogenesis and mitochondrial autophagy (mitophagy), abnormal mitochondrial dynamics (mitochondrial fusion/fission, motility, morphology, size and transport), mutations of mtDNA and so on, lead to mitochondrial dysfunction, resulting in bioenergetic defects and thus playing an important role in the pathogenesis of diseases such as neurodegenerative diseases [21–24]. As one of the best-known primary abnormalities, mitochondrial dysfunction is a distinctive early feature of AD with lower energy metabolism [25]. Mitochondrial dynamics, mitochondrial biogenesis, and mitochondrial function are impaired differently in animal models and patients of AD. Overexpression of phosphorylated tau protein in rat primary neurons reduced mitochondrial motility and caused significant mitochondrial fragmentation [26]. Abnormally fragmented mitochondria were similarly found in hippocampal and cortical sections of a transgenic AD mouse model (APP/PS1), where hyperphosphorylated tau protein could closely co-localize and bind to the mitochondrial fission protein Drp1 [27,28]. Meanwhile, phosphorylated tau protein also mediated the effect of Aβ on abnormal mitochondrial division [29]. We also found that overexpression of wild-type htau in neurons upregulated the expression of fusion proteins Mfn1, Mfn2, and Opa1, and decreased the ubiquitination modification of Mfn2 without affecting the expression of fission proteins Drp1 and Fis1, which confirmed that htau impaired mitochondrial functions by enhancing mitochondrial fusion and perinuclear aggregation [30]. However, the effects of acetylated tau in mitochondrial homeostasis and the underlying mechanism are still unclear now.

In the present study, we observed that expression of pseudoacetylated tau (TauKQ), mimicked tau acetylation at lysine residues K274 and K281, resulted in reduced mitochondrial biogenesis, decreased expression levels of mitochondrial fusion protein, and worsened mitochondrial dysfunction, therefore exacerbated cognitive ability. However, TauKR overexpression did not induce significant differences in the cognitive and mitochondrial abnormalities compared with TauWT. BGP-15 treatment ameliorated TauKQ-induced learning and memory damage via promoting mitochondrial biogenesis and improving mitochondrial dynamic homeostasis.

2. Results

2.1. Overexpressing acetyl mimetic TauKQ exacerbated cognitive impairments with neuronal loss, reduced dendritic spines and neuronal dendritic complexity

Among many potential acetylation sites in tau proteins, K274 and K281 have been detected in the human AD brains, and appear to induce mislocalization of tau, destabilization of the cytoskeleton and synaptic dysfunction [8,9,31]. To explore the role of tau acetylation in learning and memory, we constructed the acetylation mimic AAV-hSyn-EGFP-tau (Lys mutated to Gln at K274 and K281)-3flag (TauKQ), the acetylablation mimic AAV-hSyn-EGFP-tau (Lys mutated to Arg at K274 and K281)-3flag (TauKR), and the AAV-hSyn-EGFP-tau (wild-type tau)-3flag (TauWT). We stereotaxically injected the virus constructs into the dorsal hippocampal CA1 subset of 2-month-old C57 mice, respectively. After one month, the expression of hTau, enriched in hippocampal CA1, was confirmed by immunofluorescence (Fig. 1A). Meanwhile, we demonstrated by immunoprecipitation that the acetylation level of tau was significantly increased after the tau-K274/281Q mutation overexpression and decreased after the tau-K274/281R mutation overexpression (SFig. 1A and B). Since K274 and K281 can be both acetylated and ubiquitinated [32], we examined the ubiquitination level of tau by IP, but found no significant difference in tau ubiquitination after K274/281Q mutation or K274/281R mutation overexpression (SFig. 1C and D). As the most prominent symptom of AD, cognitive decline is closely associated with tau pathology [33]. Therefore, we performed behavioral tests to assess cognitive function in mice (Fig. 1B). By new object recognition (NOR) test, overexpressing three tau forms in hippocampal CA1 had no significant difference in novel object recognition preference (Fig. 1C). By Morris water maze (MWM) test, compared with the vector control, the mice overexpressing TauWT, TauKQ or TauKR showed significantly increased latency to find the hidden platform at 5th d (TauWT and TauKR), or 3rd to 5th d (TauKQ) during learning phase respectively, and TauKQ overexpression induced most serious damage in the learning ability, shown as the significantly increased latency at 4th and 5th d compared with TauWT mice. However, acetylablation mimic TauKR-overexpressed mice had better learning ability compared with TauKQ-overexpressed mice (Fig. 1D), suggesting that acetylation of tau exacerbated the impairment of learning. On day 7, the spatial memory was tested by removing the platform. A remarkably increased latency to reach the site where platform placed before, with decreased target platform crossings, and decreased time in target quadrant was shown in three hTau-expressing mice, in the meantime, acetylation mimics mutant induced the worst memory ability, and TauWT and TauKR overexpressed mice had no significant difference in memory index during the test phase (Fig. 1E–H), suggesting that tau acetylation exacerbated spatial memory deficits. No significant difference in the swimming speed among the mice in four groups was detected (Fig. 1I), which excluded defects in motor ability. In fear conditioning test, we also observed that three types of tau overexpression decreased freezing time at second day compared with the empty vector controls, and the decrease was more significant in TauKQ mice than TauWT or TauKR mice, suggesting that tau acetylation exacerbates fear memory defects (Fig. 1J and K).

A growing amount of evidences supported the neurotoxic effects of tau as a major event in neuronal loss and synaptic damage, which were both strongly associated with the severity of cognitive impairments [34–37]. To investigate the potential mechanisms of acetylation-mimics tau mutant exacerbating cognitive impairment, we detected neuron number firstly. Overexpression of Tau in the CA1 region decreased neuron numbers and increased cleaved caspase-3 level, which was more prominent while overexpression of TauKQ (Fig. 1L, M; SFig. 2A–D). By Nissl staining, in Vec group, neurons in the CA1 region had an intact and ordered shape and were closely aligned with Nissl bodies. Meanwhile, mice overexpressing three tau forms showed a reduced number of intact
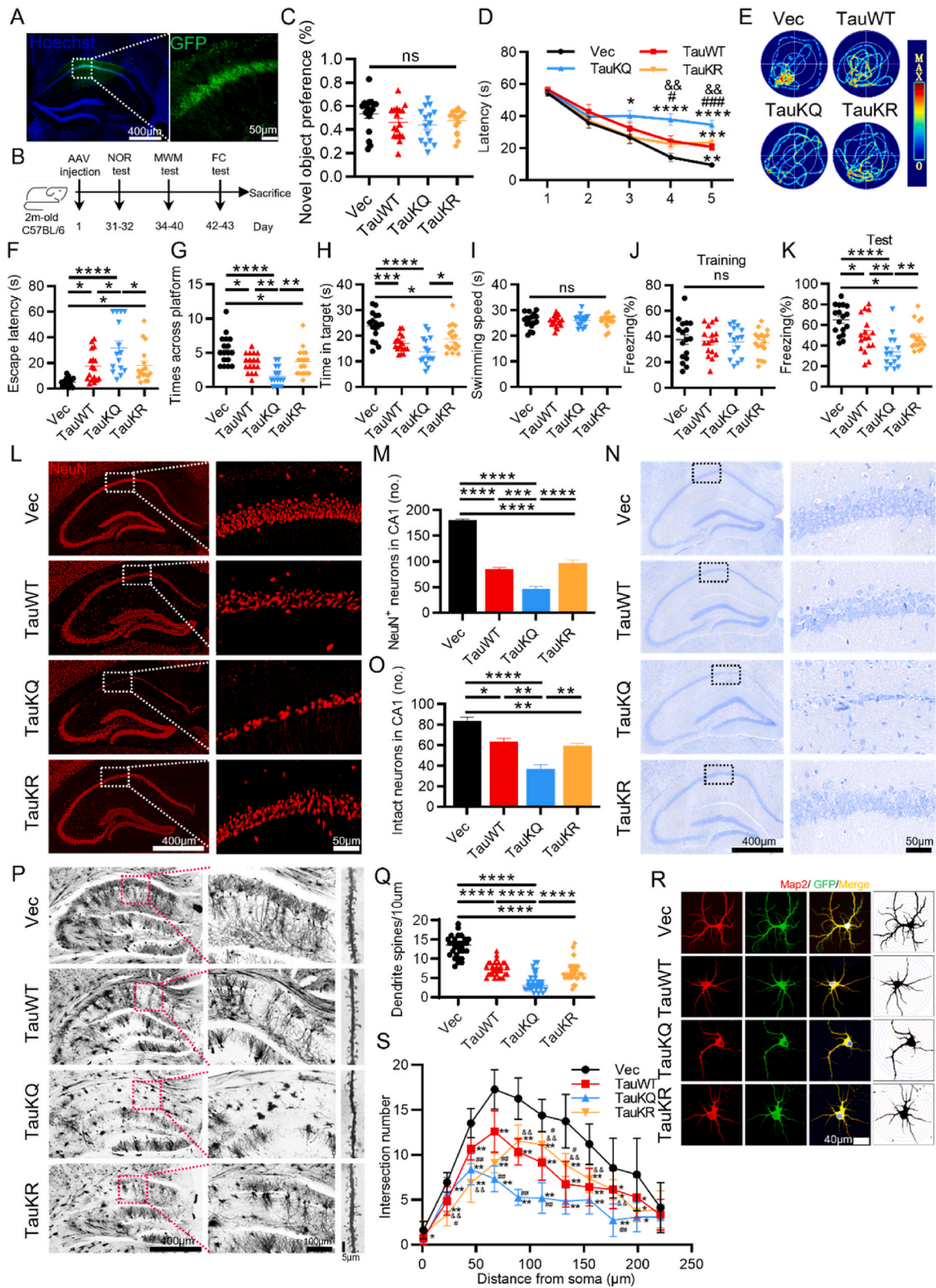
(caption on next page)

Fig. 1. Overexpressing TauKQ exacerbated cognitive impairments with neuronal loss, reduced dendritic spines, and decreased neuronal dendritic complexity. (A–K) The virus constructs including AAV-hSyn-EGFP-tau (wild-type total human tau441)-3flag (TauWT), acetylation mimic tau mutant AAV-hSyn-EGFP-tau (Lys mutated to Gln at K274 and K281)-3flag (TauKQ), the acetylablation mimic tau mutant AAV-hSyn-EGFP-tau (Lys mutated to Arg at K274 and K281)-3flag (TauKR), or the empty vector, AAV-hSyn-EGFP-MCS-3flag (Vec) were infused respectively into the hippocampal CA1 subset of 2-month-old C57 mice for one month, respectively, and then the behavior tests were carried out. (A) The expression of virus was confirmed by immunofluorescence image. (B) Experimental processes of virus injection and paradigms used for testing the cognition: NOR: Novel object recognition, MWM: Morris water maze, FC: Fear conditioning. (C) Overexpressing three tau forms in hippocampal CA1 for one month have no significant difference of novel object recognition preference (n = 15–17 mice each group). (D) During 5 days learning test by MWM, mice of TauWT, TauKQ or TauKR group showed increased latency to find the hidden platform, and the degree was more significant in mice of TaukQ than TauWT or TauKR group (n = 15–17 mice each group). (E) Representative swimming path of mice in each group during the MWM probe test. (F–I) Overexpressing all three types of tau in hippocampal CA1 for one month significantly impaired spatial memory during probe trial carried out at day 7 by removing the platform, shown as the increased latency to reach the site where the platform put before (F), the decreased crosses in the previous platform area (G) and the decreased time stayed in the target quadrant (H). No significant difference in swimming speed among four groups (I) (n = 15–17 mice each group). (J, K) In Fear conditioning (FC) test, overexpressing three tau forms in hippocampal CA1 for one month showed decreased freezing time at second day compared with the empty vector controls, the decrease was more significant in mice of TauKQ than TauWT or TauKR group (n = 15–17 mice each group). (L, M) Representative images of NeuN immunofluorescence staining (L), and the quantitative analysis (M) (n = 3 from three independent experiments). (N, O) Representative images of Nissl staining (N), and the quantitative analysis. Neurons with visible nuclei, distinctive nucleolus, and cytoplasmic Nissl staining were regarded as intact neurons and counted (O) (n = 3 from three independent experiments). (P, Q) Representative images of Golgi Staining in the hippocampus of mice (P). Quantitative analysis of spine density in the CA1 subset of mice. 30 neurons from three mice per group were analyzed. (R, S) The primary cultured hippocampal neurons were infected with the lenti-TauWT, lenti-TauKQ, lenti-TauKR, or lenti-vector-EGFP (Vec) at 2 div (days in vitro). Neurons were stained using anti-MAP2 antibody and the dendrite complexity was analyzed at 8 div. The representative images show changed dendrite complexity by overexpressing all three types of tau in cultured hippocampal neurons at 8 div (R). Sholl analyses of the numbers of dendritic crossings in hippocampal neurons (S). 15 neurons from six independent cultures were analyzed for each group.

All data were presented as mean ± SEM. Two-way repeated measures ANOVA test followed by Tukey's post hoc test for D and S, and One-way ANOVA test followed by Tukey's post hoc test for others. D and S: *, $p < 0.05$, **, $p < 0.01$, ***, $p < 0.001$, ****, $p < 0.0001$, vs Vec; #, $p < 0.05$, ##, $p < 0.01$, ###, $p < 0.001$, vs TauWT; &&, $p < 0.01$, vs TauKQ. Others: *, $p < 0.05$, **, $p < 0.01$, ***, $p < 0.001$, ****, $p < 0.0001$.

neurons (Fig. 1N and O), with abnormal morphology, blurred structure and disorganized arrangement (Fig. 1N), which were most apparent in the TauKQ mice (Fig. 1N and O). We also observed that the dendritic spines of neurons in the CA1 area were significantly reduced after overexpressing tau, and TauKQ overexpression induced a more significant reduction by Golgi staining (Fig. 1P and Q). In order to further observe the effect of tau acetylation on dendritic plasticity, lentiviruses separately expressing three different types of tau or the empty vector were transfected into primary cultured hippocampal neurons at 2 div, by staining dendrites with anti-MAP2 at 8 div, Sholl analysis showed that overexpressing any one of the three types of tau made the dendrite branches of neurons reduced, among them the most pronounced one is the TauKQ (Fig. 1R and S). The above results indicate that the mimic acetylation of tau at K274/K281 led to aggravating learning and memory impairment in mice, with loss of neurons, decreased dendritic spines, and reduced dendritic complexity of neurons.

2.2. Overexpressing TauKQ exacerbated mitochondrial dysfunction

Neurons heavily depend on mitochondria to meet the energy demand for synaptic transmission. To further study the underlying mechanisms of aggravation of neuronal damage and synaptic loss induced by acetylation mimic tau mutant, we first examined the effect of tauKQ on the mitochondrial function. We found that overexpression of human tau in primary cultured neurons decreased both ATP levels and the ratio of ATP/ADP, as well as inhibition of complex I activity [30], so we conjectured that acetylated tau may induce more negative effects on mitochondria than TauWT, as it induced much more serious neuronal damage. First, by examining multi-subunit complexes I, II and III, and ATP synthase (complex V) of the mitochondrial electron transport chain, we found that overexpression of TauKQ significantly decreased mitochondrial complex I and II, and the other complex also showed a clear trend toward decrease, although this trend had no statistical significance. TauWT and TauKR only decreased mitochondrial complex I (Fig. 2A and B). ATP level also significantly reduced, which was more prominent in the TauKQ group (Fig. 2C). The total SOD activity was higher in the TauWT and TauKR mice than the control, but had no change in TauKQ mice (Fig. 2D). To further explore the effect of tau acetylation on mitochondrial function, we transfected lentiviruses (TauWT, TauKQ, and TauKR) into primary hippocampal neurons to examine the intracellular (detected by DCFH-DA) and the mitochondrial ROS (detected by MitoSOX) production and mitochondrial membrane

potential (detected by TMRE) level. We observed that, overexpression of three tau forms resulted in intracellular and mitochondrial ROS production increase (Fig. 2E–H) and mitochondrial membrane potential impairment (Fig. 2I and J), which were most pronounced when infected with TauKQ viruses. The above results suggested that acetylation of tau at K274/K281 exacerbated mitochondrial dysfunction.

2.3. Overexpressing TauKQ reduced mitochondrial biogenesis

Then, we investigated the mechanisms by which the acetylation mimic tau mutant deteriorates mitochondrial dysfunction. Firstly, we detected the proteins related to mitochondrial biogenesis, including peroxisome proliferator-activated receptor-γ coactivator 1 alpha (PGC-1α), nuclear respiratory factor 1 (Nrf1), and mitochondrial transcription factor A (Tfam) [38], whose expression was significantly reduced in neurodegenerative diseases such as AD, suggesting reduced mitochondrial biogenesis [25]. Overexpressing TauKQ reduced PGC-1α, Nrf1 and Tfam in primary cultured hippocampal neurons and the hippocampal CA1 region of mice (Fig. 3A–D), TauKR or TauWT increased PGC-1α and Nrf1 levels compared with TauKQ, while it had no significant difference when compared with the vector control in vitro and in vivo. The mitochondrial outer membrane protein Tomm40 expression was also increased in the TauWT and TauKR groups, though acetylated tau reversed this, this was possibly due to the reduced mitochondrial biogenesis (Fig. 3A–D). Autophagy marker LC3 (microtubule-associated protein 1 light chain 3)-II and P62 (SQSTM1) were also increased by overexpressing TauWT, TauKQ or TauKR (Fig. 3A–D), this imply that autophagy was impaired [39]. Real-time PCR suggested a significant decrease in the mRNA level of PGC-1α, Nrf1, or Tfam after TauKQ overexpression (Fig. 3E). To further verify whether mitochondrial biogenesis is damaged, we measured mtDNA relative to nDNA (mtDNA/nDNA). It was found that mtDNA/nDNA was increased in the TauWT and TauKR mice, while decreased in TauKQ mice, which suggested that mitochondria biogenesis was inhibited by acetyl-mimic tau mutant (Fig. 3F).

2.4. Overexpressing TauKQ disrupted mitochondrial dynamics by reducing mitochondrial fusion

Mitochondria are highly dynamic organelles undergoing coordinated cycles of fission and fusion, referred as 'mitochondrial dynamics', in order to maintain their shape, distribution and size [40]. After
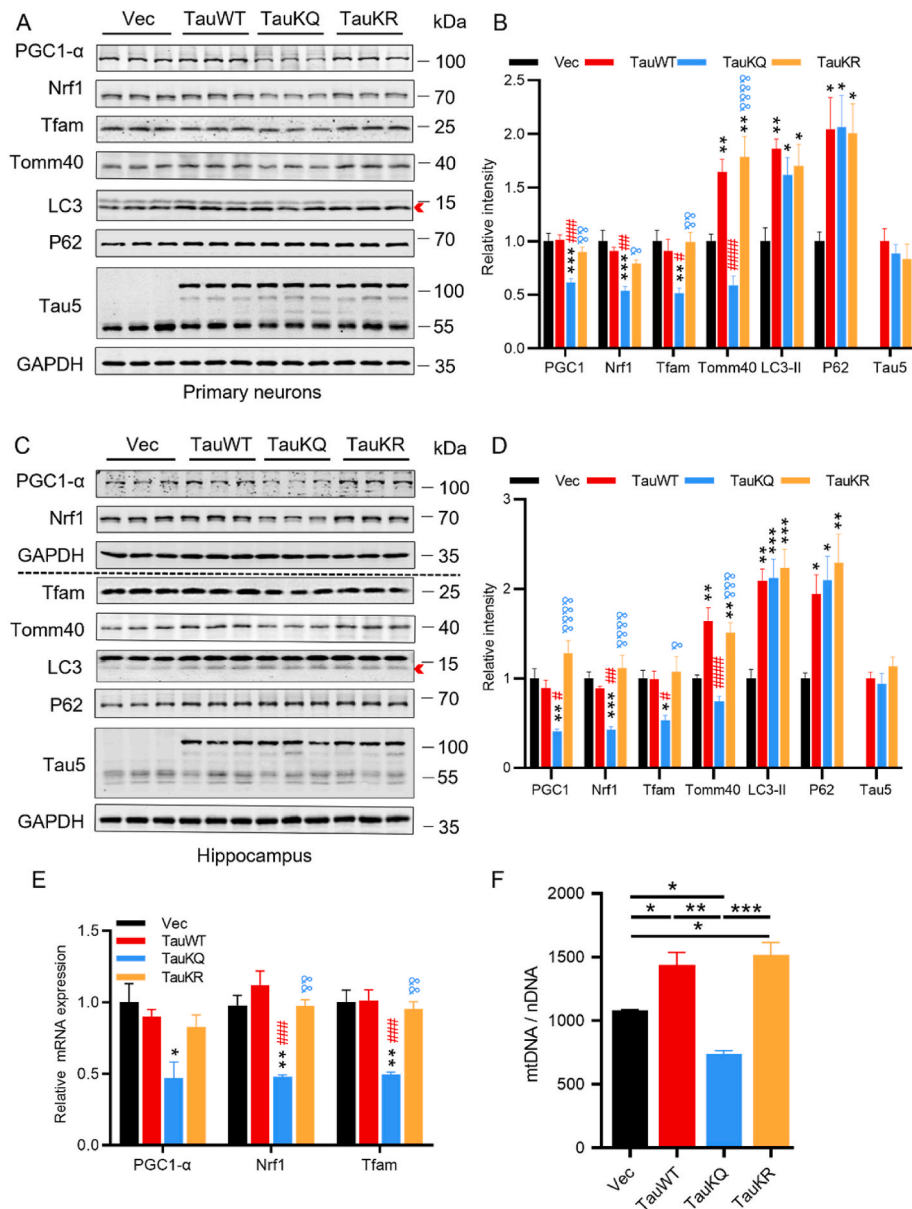
Fig. 2. Overexpressing TauKQ exacerbated mitochondrial dysfunctions. (A, B) The expression levels of mitochondrial respiratory complex I (NDUFB8), II (SDHB), III (UQCRC2), V (ATP5A) protein and total Tau (Tau5) were detected by Western blotting (A) and quantitative analysis (B) (n = 6 biological replicates each group). (C) The change of ATP level in four groups of mice (n = 5 biological replicates each group). (D) The change of total SOD activity in four groups of mice (n = 6 biological replicates each group). (E, F) The primary cultured hippocampal neurons were infected with the lenti-TauWT, lenti-TauKQ, lenti-TauKR, or lenti-vector-EGFP (Vec) at 2 div, stained with DCFH-DA (red) at 8 div. The image showing the intracellular ROS levels after the indicated treatments (E), and the quantification of relative ROS level (red) (F) (n = 6 each group). (G, H) The primary cultured hippocampal neurons were infected with the lenti-TauWT, lenti-TauKQ, lenti-TauKR, or lenti-vector-EGFP (Vec) at 2 div, stained with MitoSOX (red) at 8 div. The image showing the mitochondrial ROS levels after the indicated treatments (G), and the quantification of relative ROS level (red) (H) (n = 6 each group). (I, J) The primary cultured hippocampal neurons were infected with the lenti-TauWT, lenti-TauKQ, lenti-TauKR, or lenti-vector-EGFP (Vec) at 2 div, stained with TMRE (red) at 8 div. The image showing the mitochondrial membrane potential (MMP) in neurons with indicated treatments (I), and the quantification of relative MMP level (red) (J) (n = 6 each group).

All data were presented as mean ± SEM. One-way ANOVA test followed by Tukey's post hoc test. *, $p < 0.05$, **, $p < 0.01$, ***, $p < 0.001$, ****, $p < 0.0001$. (For interpretation of the references to colour in this figure legend, the reader is referred to the Web version of this article.)

Fig. 3. Overexpressing TauKQ attenuated mitochondrial biogenesis. (A, B) The expression levels of mitochondrial biogenesis pathway proteins, such as PGC-1α, Nrf1 and Tfam, autophagy-related proteins p62, LC3, the mitochondrial outer membrane protein Tomm40, and total Tau (Tau5) were detected by Western blotting (A) and quantitative analysis (B) in primary cultured hippocampal neurons with expression of all three types of tau lentivirus. For the quantification of LC3, we used LC3-II, the band marked by the arrow (n = 6 biological replicates each group). (C, D) The protein expression levels of PGC-1α, Nrf1, Tfam, Tomm40, LC3, P62 and total Tau (Tau5) were detected by Western blotting (C) and quantitative analysis (D) in hippocampal CA1 extracts of the three types of tau overexpressing mice. For the quantification of LC3, we used LC3-II, the band marked by the arrow (n = 6 biological replicates each group). (E) The mRNA expression levels of PGC-1α, Nrf1, and Tfam were detected by qRT–PCR in the hippocampal CA1 of the three types of tau overexpressing mice. The fold change was normalized with the loading control GAPDH and expressed relative to the Vec group (n = 3–5 each group). (F) The change of relative mtDNA copy number (mtDNA/nDNA) in hippocampal CA1 of the four groups mice detected by qRT-PCR (n = 3 each group).

All data were presented as mean ± SEM. One-way ANOVA test followed by Tukey's post hoc test. B, D and E: *, $p < 0.05$, **, $p < 0.01$, ***, $p < 0.001$, vs Vec; #, $p < 0.05$, ##, $p < 0.01$, ###, $p < 0.001$, ####, $p < 0.0001$, vs TauWT; &, $p < 0.05$, &&, $p < 0.01$, &&&, $p < 0.001$, &&&&, $p < 0.0001$, vs TauKQ. F: *, $p < 0.05$, **, $p < 0.01$, ***, $p < 0.001$.

overexpressing TauWT in primary cultured hippocampal neurons, we observed that the expression of mitochondrial fusion protein Mfn1, Mfn2, and Opa1 increased, while mitochondrial fission proteins Fis1 and Drp1 had no change, which was consistent with our previous study in the htau-expressing HEK293 cells and htau transgenic mice [30]. However, overexpression of TauKQ significantly reduced Mfn1, Mfn2 and Opa1 levels compared with the Vec or TauWT group, while TauKR overexpression increased Mfn1, Mfn2 and OPA1 levels compared with the TauKQ group, accompanied with the increased Mfn1 and Mfn2 level compared with the Vec group (Fig. 4A and B). After transfection with three types of tau, mitochondria were labeled by MitoTracker Red at 8 div. We found that overexpression of TauWT and TauKR significantly increased mitochondrial length, while mitochondrial length was significantly reduced after overexpression of TauKQ (Fig. 4C and D). Compared with the Vec group, overexpression of TauWT in the hippocampal CA1 region increased the mRNA and protein levels of Mfn1, Mfn2 and Opa1, and overexpressing TauKR increased Mfn1 and Opa1, while TauKQ significantly reduced these fusion proteins (Fig. 4E–G). The mitochondrial fission proteins had no significant change in vitro and in vivo (Fig. 4A, B, E, F, G). To further confirm the effect of acetylated

tau on mitochondrial dynamics, we detected mitochondrial morphology by electron microscopy. The morphology of mitochondria was divided into four categories based on the value of mitochondria length/diameter (L/D), and the mitochondria were divided into three categories based on the degree of loss of cristae [41]. We observed that mitochondrial elongation (the ratio of mitochondria length/diameter is more than 4.5) was account for a large proportion with loss of a small number of cristae in neurons of the hippocampal CA1 region in TauWT and TauKR mice, whereas TauKQ induced mitochondria fragmented (the ratio of mitochondria length/diameter equal to 1–1.5), and mitochondria morphology became rounded and swollen, and mitochondrial cristae were severely lost and appeared vacuolated (Fig. 4H–J).

All the above data suggested that tau acetylated at K274/K281 aggravated mitochondrial dysfunction by disrupting the dynamic homeostasis (promoting mitochondria fission) and inhibiting mitochondrial biogenesis, which in turn led to neuronal loss and dendritic spine damage.
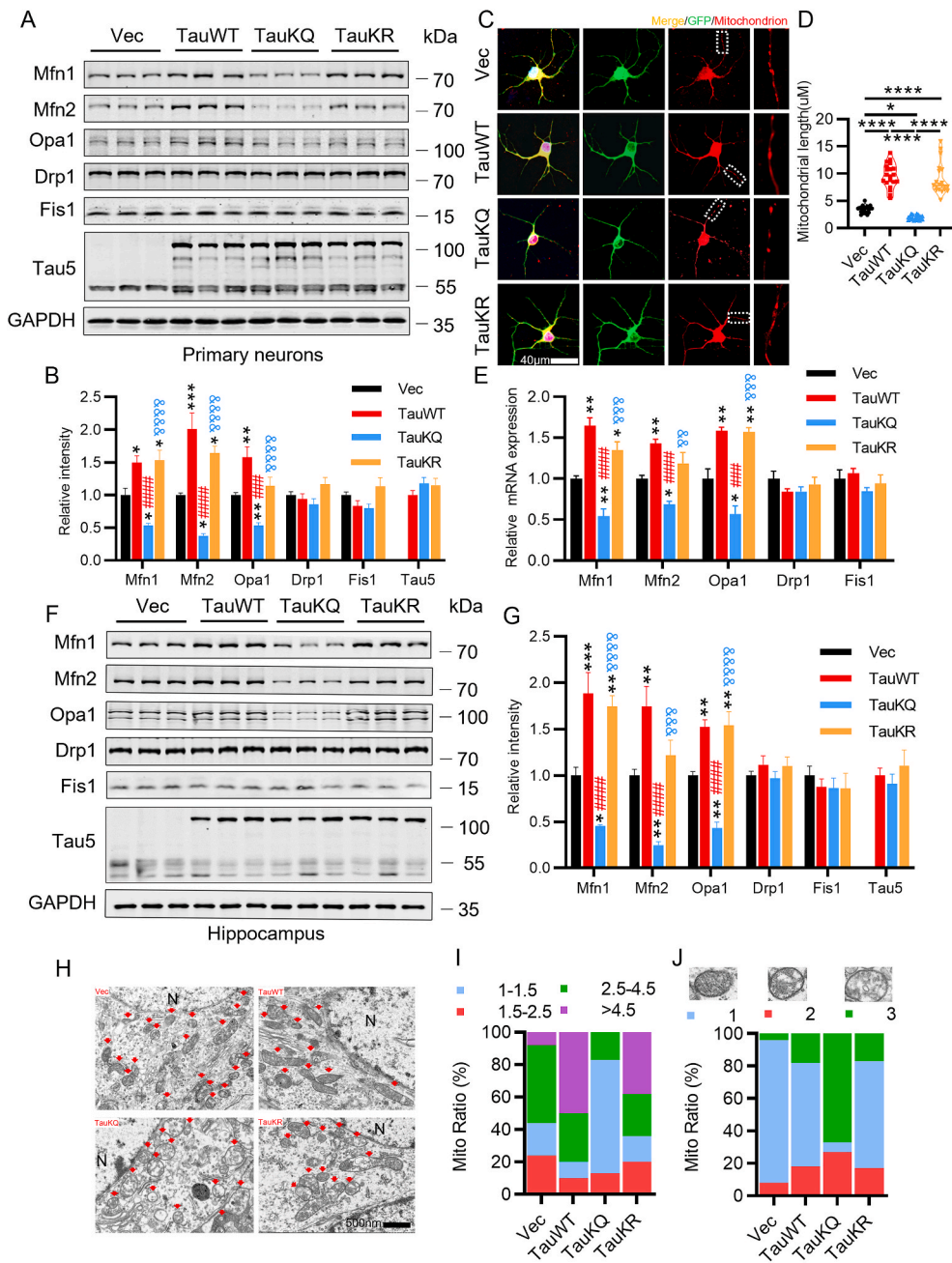
Fig. 4. Overexpression of TauKQ disrupted mitochondrial dynamics by reducing mitochondrial fusion. (A, B) The expression levels of mitochondrial dynamic proteins were detected by Western blotting (A) and quantitative analysis (B) in primary cultured hippocampal neurons with expression of three types of tau lentivirus (n = 6 biological replicates each group). (C, D) The primary cultured hippocampal neurons were infected with three types of tau lentivirus at 2 div. Mitochondria were labeled by MitoTracker Red at 8 div. The representative images were shown (C). The mitochondrial length (counted in the neuronal processes 100–200 μm away from the cell body) were measured and quantified (D). 15–20 neurons from six independent cultures were analyzed for each group. (E) Overexpression of three types of tau changed the mRNA levels of Mfn1, Mfn2, and Opa1 in the hippocampal CA1 detected by qRT-PCR (n = 3 each group). (F, G) Overexpression of three types of tau changed the protein levels of Mfn1, Mfn2, and Opa1 in the hippocampal CA1, detected by Western blotting (n = 6 biological replicates each group). (H–J) Overexpression of three types of tau changed the mitochondrial morphology detected by electron microscopy in the hippocampal CA1 subset. Typical mitochondrial images were presented (H). N, nucleus; arrow, mitochondria. The morphology of mitochondria was divided into four categories based on the value of mitochondria length/diameter (L/D), and the proportion of each category is shown (I). The mitochondria were divided into three categories based on the cristae morphology (blue, intact; red, a slight loss of cristae; and green, a severe loss of cristae). The proportion of each type of mitochondria is shown (J). At least 100 mitochondria from three mice per group were analyzed.

All data were presented as mean ± SEM. One-way ANOVA test followed by Tukey's post hoc test. B, E and G: *, $p < 0.05$, **, $p < 0.01$, ***, $p < 0.001$, vs Vec; ###, $p < 0.001$, ####, $p < 0.0001$, vs TauWT; &&, $p < 0.01$, &&&, $p < 0.001$, &&&&, $p < 0.0001$, vs TauKQ. D: *, $p < 0.05$, ****, $p < 0.0001$. (For interpretation of the references to colour in this figure legend, the reader is referred to the Web version of this article.)

2.5. BGP-15 rescued TauKQ-induced injury in mitochondrial biogenesis

BGP-15 is a hydroxylamine derivative that has been shown to exert cyto- and neuroprotective effects in a wide range of models in vivo and in vitro [42–56], with involving the mechanisms of increasing mitochondrial fusion proteins and promoting mitochondrial biogenesis through PGC-1α signaling pathway [57,58]. Next, we aimed to investigate whether BGP-15 attenuated TauKQ-induced mitochondrial damage. In primary cultured hippocampal neurons infected with lenti-TauKQ, PGC1-α, Nrf1, Tfam were significantly decreased, and then BGP-15 treatment reversed the decreased PGC1-α, Nrf1 and Tfam with a significant increase of Tomm40 (Fig. 5A and B). The same results were also obtained in vivo (Fig. 5C and D). At the same time, the reduction of mtDNA copy number caused by TauKQ was also rescued by BGP-15 (Fig. 5E). Treatment with BGP-15 alone did not alter the levels of PGC1-α, Nrf1, Tfam, Tomm40 and mtDNA copy number in vivo

and/or in vitro (Fig. 5A–E).

2.6. BGP-15 improved mitochondrial dynamic homeostasis by rescuing TauKQ-induced mitochondrial fission

We examined the effects of BGP-15 treatment on mitochondrial dynamic homeostasis. When treated with BGP-15 alone, mitochondrial fusion protein Mfn2 and fission protein Drp1 were significantly increased in primary hippocampal neurons. Overexpression of TauKQ resulted in a significant decrease in Mfn1, Mfn2 and Opa1 levels, while BGP-15 reversed these to the similar level of the Vec, at the same time, we also observed an increase in Drp1 (Fig. 6A and B). Labeling mitochondria with MitoTracker Red, we observed that BGP-15 rescued TauKQ-induced mitochondrial fission, presented as the average mitochondria length increased from ~2 to ~4 μm (Fig. 6C and D). In vivo, BGP-15 treatment reversed the decreased Mfn1, Mfn2 and Opa1 levels
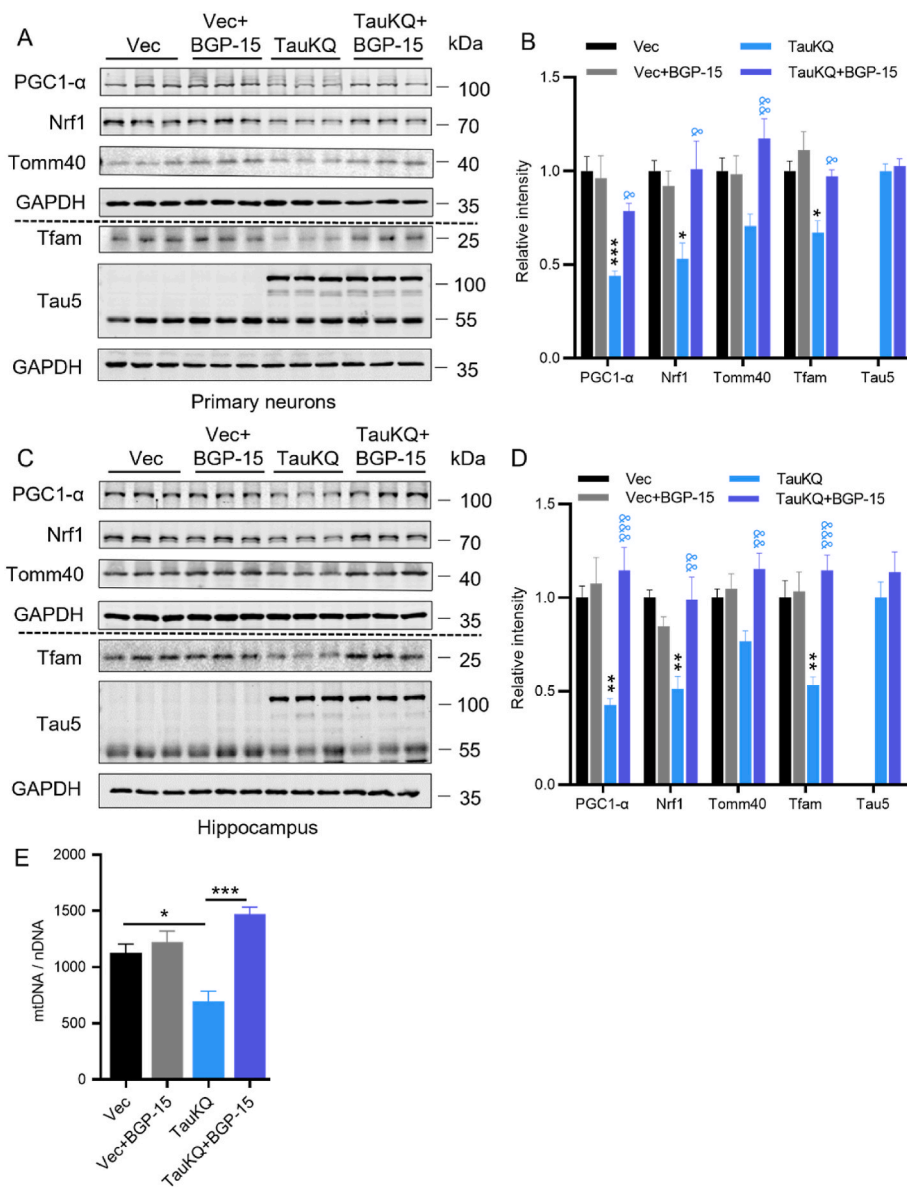
Fig. 5. BGP-15 rescued TauKQ-induced reduction in mitochondrial biogenesis. (A, B) BGP-15 rescued TauKQ-induced reduction in PGC1-α/Nrf1/Tfam in primary cultured hippocampal neurons. After infected with the lenti-tau (Lys mutated to Gln at K274 and K281)-EGFP (TauKQ)at 2 div, the primary cultured hippocampal neurons were treated with 10 μM BGP-15 at 3 div for 5 d, half-change the culture medium every other day until sample collection at 8 div. The expression levels of PGC1-α, Nrf1, Tfam, Tomm40 and total Tau (Tau5) were detected by Western blotting (A) and quantitative analysis (B) (n = 6 biological replicates each group). (C, D) BGP-15 rescued TauKQ-induced reduction in PGC1-α/Nrf1/Tfam in the hippocampal CA1 subset. The virus constructs including AAV-hSyn-EGFP-tau (Lys mutated to Gln at K274 and K281)-3flag (TauKQ) was infused into the hippocampal CA1 subset of 2-month-old C57 mice for 20 d, followed by daily oral BGP-15 (28 mg/kg) for 10 d. The expression levels of PGC-1α, Nrf1, Tfam, Tomm40 and total Tau (Tau5) were detected by Western blotting (C) and quantitative analysis (D) (n = 6 biological replicates each group). (E) BGP-15 increased mtDNA copy number (mtDNA/nDNA) in the hippocampal CA1 subset of TauKQ-expressing mice. The relative mtDNA copy number detected by qRT-PCR (n = 3 each group).

All data were presented as mean ± SEM. One-way ANOVA test followed by Tukey's post hoc test. B and D: *, $p < 0.05$, **, $p < 0.01$, ***, $p < 0.001$, vs Vec; &, $p < 0.05$, &&, $p < 0.01$, &&&, $p < 0.001$, vs TauKQ. E: *, $p < 0.05$, ***, $p < 0.001$.

caused by TauKQ (Fig. 6E and F). Meanwhile, BGP-15 treatment reversed proportion of fragmented mitochondria (the ratio of mitochondria length/diameter equal to 1–1.5) caused by TauKQ, reduced loss of mitochondrial cristae, decreased vacuolization, and increased internal mitochondrial densities (Fig. 6G–I).

2.7. BGP-15 ameliorated TauKQ-induced mitochondrial dysfunction

The changes in mitochondrial biogenesis and mitochondrial dynamics are finally reflected in the altered mitochondrial function [59]. To investigate the effect of BGP-15 on TauKQ-induced mitochondrial dysfunction, by DCFH-DA, MitoSOX and TMRE staining in primary hippocampal neurons, we observed that increased intracellular and mitochondrial ROS induced by overexpressing TauKQ was attenuated by BGP-15 treatment (Fig. 7A–D) and the mitochondrial membrane potential was also increased (Fig. 7E and F). Meanwhile, the impaired mitochondrial ATP production was ameliorated by BGP-15 treatment (Fig. 7G), but the total SOD activity did not change significantly (Fig. 7H).

The above results suggested that BGP-15 attenuated the decreased mitochondrial biogenesis and disruption of mitochondrial dynamic

homeostasis induced by TauKQ overexpression, thereby rescuing mitochondrial dysfunction.

2.8. BGP-15 rescued cognitive impairment by amelioration of neuronal loss and dendritic spine reduction, and increased neuronal dendritic complexity

Lastly, we further explored whether BGP-15 improved the cognitive deficits induced by TauKQ. By MAP2 immunofluorescence staining in primary cultured hippocampal neurons, we observed that the dendritic complexity of neurons was significantly ameliorated (shorter dendrite length and fewer dendritic crossings) by TauKQ overexpression, while it was reversed after BGP-15 treatment (Fig. 8A and B). By NeuN immunofluorescent staining and Nissl's staining, we observed that BGP-15 treatment alone had no effects in neuron number, whereas the decreased neuron number induced by overexpressing TauKQ was reversed by BGP-15 treatment in the hippocampal CA1 region of mice (Fig. 8C–F). Furthermore, both in vitro and in vivo, BGP-15 treatment attenuated the increased cleaved caspase-3 levels induced by TauKQ, thus indicating that BGP-15 alleviated TauKQ-induced neuronal apoptosis (SFig. 3A–D). The Golgi staining showed that the dendritic
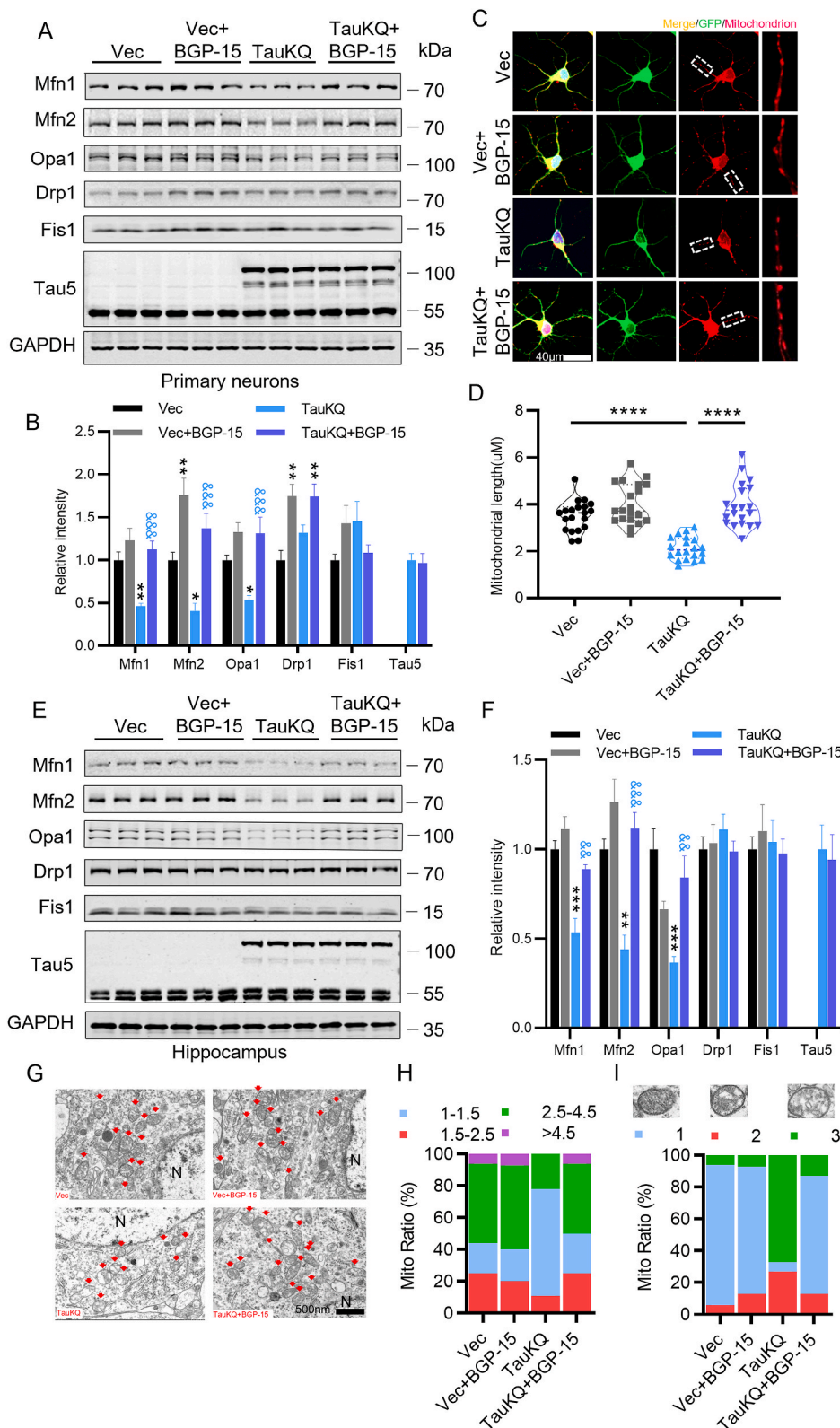
Fig. 6. BGP-15 reversed TauKQ-induced mitochondrial dynamic imbalance. (A, B) BGP-15 rescued TauKQ-induced reduction of mitochondrial fusion-associated proteins in primary hippocampal neurons. The expression levels of Mfn1, Mfn2, Opa1, Drp1, Fis1 and total Tau (Tau5) were detected by Western blotting (A) and quantitative analysis (B) (n = 6 biological replicates each group). (C, D) BGP-15 rescued TauKQ-induced mitochondrial fragmentation in primary hippocampal neurons. The representative images were shown (C). The mitochondrial length (counted in the neuronal processes 100–200 μm away from the cell body) were measured and quantified (D). 15–20 neurons from six independent cultures were analyzed for each group. (E, F) BGP-15 rescued TauKQ-induced reduction of mitochondrial fusion-associated proteins in the hippocampal CA1 subset. The expression levels of Mfn1, Mfn2, Opa1, Drp1, and Fis1 and total Tau (Tau5) were detected by Western blotting (E) and quantitative analysis (F) (n = 6 biological replicates each group). (G–I) BGP-15 treatment ameliorated the mitochondrial morphology in the hippocampal CA1 neurons of C57 mice detected by electron microscopy. Typical mitochondrial images were presented (G). N, nucleus; arrow, mitochondria. The morphology of mitochondria was divided into four categories based on the value of mitochondria length/diameter (L/D). The proportion of each category is shown (H). The mitochondria were divided into three categories based on the cristae morphology (blue, intact; red, a slight loss of cristae; and green, a severe loss of cristae). The proportion of each type of mitochondria inside the neurons of hippocampal CA1 is shown (I). At least 100 mitochondria from three mice per group were analyzed. All data were presented as mean ± SEM. One-way ANOVA test followed by Tukey's post hoc test. B and F: *, $p < 0.05$, **, $p < 0.01$, ***, $p < 0.001$, vs Vec; &&, $p < 0.01$, &&&, $p < 0.001$, vs TauKQ. D: ****, $p < 0.0001$. (For interpretation of the references to colour in this figure legend, the reader is referred to the Web version of this article.)

branches of TauKQ group were severely disrupted and the density of dendritic spines was significantly reduced. Meanwhile, BGP-15 treatment attenuated the phenotype in TauKQ mice (Fig. 8G and H). Finally, we conducted behavioral tests to assess cognitive ability. There was no significant difference of novel object recognition preference among the four groups mice (Fig. 8I). By MMW test, we found that BGP-15

improved learning and memory abilities in TauKQ mice shown by shorten latency to find the hidden platform during training stage (Fig. 8J), the decreased latency to reach the site where platform put before, the increased crossing time in the previous platform area and the more time stayed in the target quadrant during test phase (Fig. 8K-N). There was no significant difference in swimming speed among the four
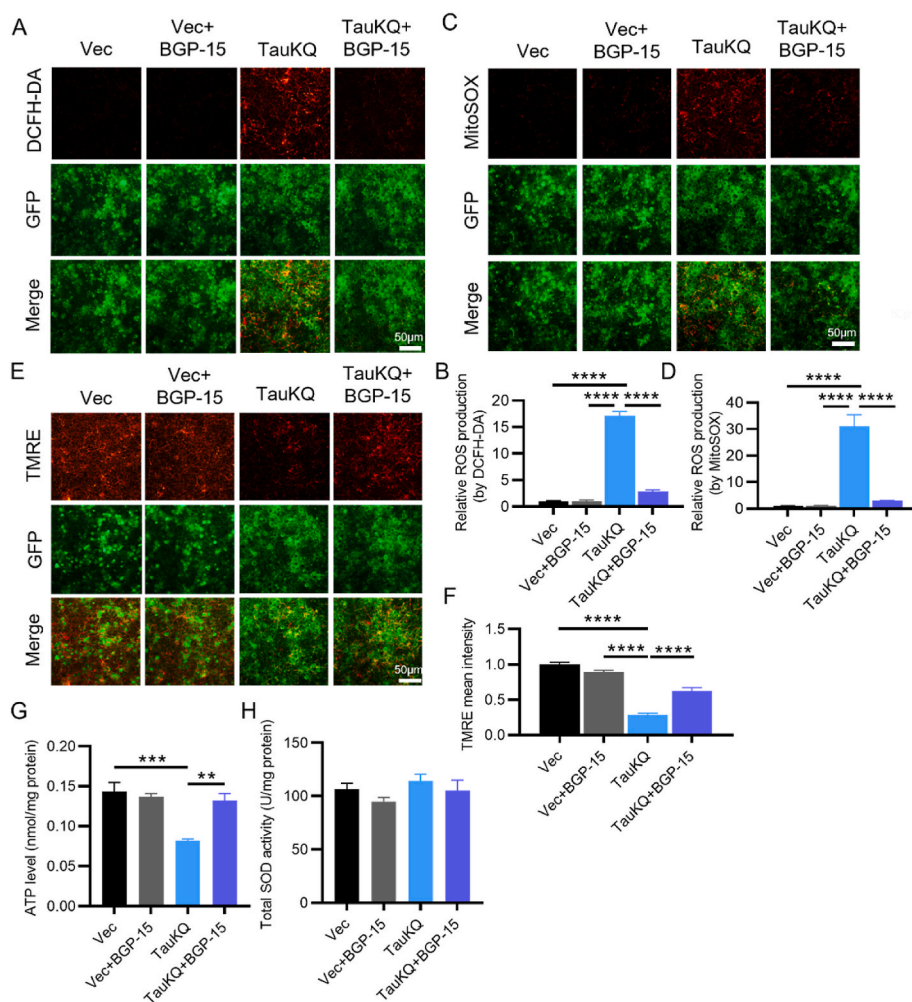
Fig. 7. BGP-15 ameliorated TauKQ-induced mitochondrial dysfunctions. (A, B) BGP-15 decreased TauKQ-induced intracellular ROS level in primary hippocampal neurons. The present image showing the intracellular ROS levels (red) in primary neurons after the indicated treatments (A). The quantification of relative intracellular ROS generation (B) (n = 6 each group). (C, D) BGP-15 decreased TauKQ-induced mitochondrial ROS level in primary hippocampal neurons. The present image showing the mitochondrial ROS levels (red) in primary neurons after the indicated treatments (C). The quantification of relative mitochondrial ROS generation (D) (n = 6 each group). (E, F) BGP-15 prevented TauKQ-induced MMP (red) reduction in primary hippocampal neurons. The representative image after indicated treatments (E). The quantification of relative MMP (F) (n = 6 each group). (G) BGP-15 treatment reversed the decreased ATP levels in TauKQ-expressing mice (n = 4–5 biological replicates each group). (H) BGP-15 treatment did not affect the total SOD activity (n = 5 biological replicates each group).

All data were presented as mean ± SEM. One-way ANOVA test followed by Tukey's post hoc test. **, $p < 0.01$, ***, $p < 0.001$, ****, $p < 0.0001$. (For interpretation of the references to colour in this figure legend, the reader is referred to the Web version of this article.)

groups of mice (Fig. 8O), which excluded defects in motor ability. In fear conditioning (FC) test, BGP-15 rescued fear memory defects, which were shown by an increased freezing time during memory test (Fig. 8P and Q). These data suggested that BGP-15 ameliorated TauKQ-induced cognitive deficits.

3. Discussion

Tau isolated from AD brain tissue exhibits many post-translational modifications (PTM), of which phosphorylation is the most prevalent and well-studied. Recently, there are growing evidences that tau is also aberrantly acetylated. Acetylated tau at the K274 and K281 sites remarkably increased in the early stages of AD, and more significantly increased in the brains of advanced AD patients with severe dementia [9, 17]. There are continuing evidences that human total or phosphorylated tau expression in AD animal models leads to mitochondrial dysfunction [60]. However, the effects and the mechanisms of acetylated tau protein on mitochondria functions have not been well studied until now. In the present study, we firstly reported that, tau acetylated at K274/K281 (TauKQ) had more severe neurotoxicity than wild type and non-acetylated tau. It induced mitochondrial dysfunction by reducing mitochondrial biogenesis and disturbing mitochondrial dynamic balance, and thus causing cognitive deficits. We also found that BGP-15 reversed TauKQ induced mitochondrial dysfunctions and cognitive deficits by promoting mitochondrial biogenesis and fusion.

Mitochondrial abnormalities with energy metabolism defects were an early and prominent feature of AD [61–63]. Mitochondrial homeostasis is maintained by the coordination of pathways like mitochondrial biogenesis, dynamics, and degradative pathways, such as the activation of mitochondrial proteases, mitochondrial-derived vesicles, and mitophagy, the selective degradation of mitochondria via autophagy [64]. Increased biogenesis is compatible with the mtDNA copy number and enhanced mitochondrial gene expression [38]. Here, from three aspects: mitochondrial biogenesis, dynamics (fission and fusion) and degradation (mitophagy), we found that the damage induced by tau acetylation was the most severe one, although three tau forms all induced mitochondrial dysfunctions. In the present study, overexpression of htau resulted in impaired mitophagy by showing increased LC3-II, P62, and Tomm40, which was consistent with our previous studies [39,65]. However, overexpression of TauKQ not only resulted in impaired mitophagy, but also decreased mitochondrial biogenesis, which exacerbated TauKQ-induced mitochondrial dysfunctions and cognitive defects. It had also been evidenced that there was a significant decrease in the mitochondrial production pathway PGC1-α/Nrf1/TFAM and the mitochondrial copy number mtDNA in AD human brain [25,66, 67], which was consistent with our results with TauKQ overexpression. Additionally, Tfam plays an important role in the maintenance of mtDNA integrity [68], so in addition to controlling the biogenesis of mitochondria, the decrease of Tfam in our TauKQ-expressing mice may also aggravate the dysfunction of mitochondria in another way. Though mtDNA decreased, mitochondrial marker Tomm40 level had no change compared with the wt mice. One possibility of this phenomenon is the inhibition of the degradation of mitochondria (mitophagy).

Mitochondria are highly dynamic organelles undergoing continuous
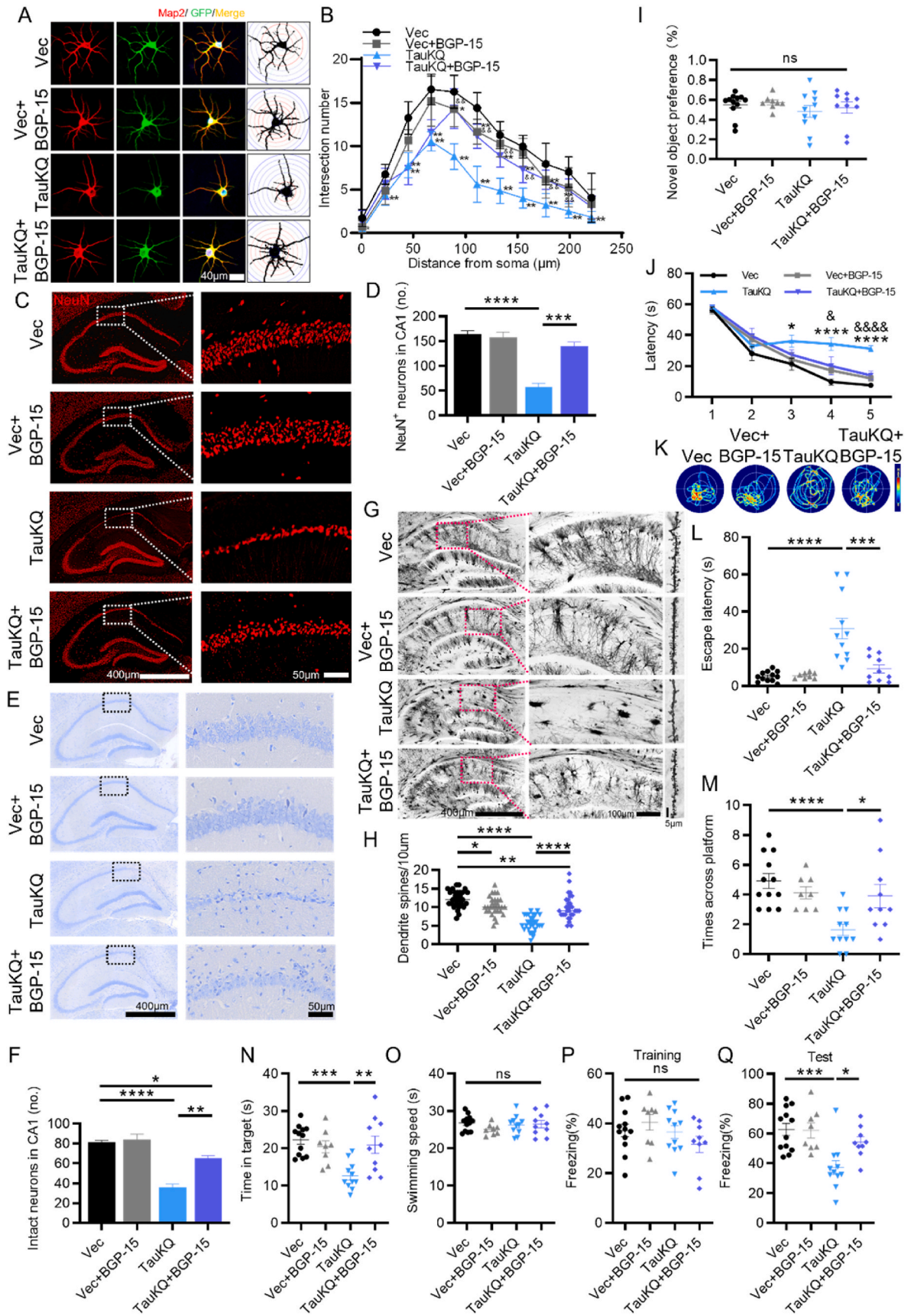
(caption on next page)

Fig. 8. BGP-15 ameliorated TauKQ-induced learning and memory impairments, with rescuing neuronal loss and dendritic spine reduction, and increasing neuronal dendritic complexity. (A, B) The primary cultured hippocampal neurons were infected with the lenti-tau (Lys mutated to Gln at K274 and K281)-EGFP (TauKQ) at 2 div, and thus treated with 10 μM BGP-15 at 3 div. Neurons were stained using anti-MAP2 at 8 div and the dendrite complexity was analyzed. The representative images of dendrite complexity (A). Sholl analyses showed that the number of dendrite crossings was reduced by overexpressing TauKQ, and BGP-15 reversed the reduction (B). 20 neurons from six independent cultures were analyzed for each group. (C, D) BGP-15 ameliorated hippocampal CA1 neuronal loss in TauKQ-expressing mice, exhibited by representative images of NeuN immunofluorescence staining (C). Quantitative analysis for the number of neurons with NeuN staining in area framed within white bordered rectangle (D) (n = 3 from three independent experiments). (E, F) Representative images of Nissl staining (E), and quantitative analysis (F) (n = 3 from three independent experiments). (G, H) Representative images of Golgi Staining in the hippocampal of mice (G), and quantitative analysis of spine density in the CA1 area of mice (H). 30 neurons from three mice per group were analyzed. (I–Q) The AAV-TauKQ were infused respectively into the hippocampal CA1 subset of 2-month-old C57 mice for 20 d, followed treatment with BGP-15 (28 mg/kg/d) by gavage for 10 d. (I) There was no significant difference of novel object recognition preference among the four groups mice detected by NOR test (n = 8–12 mice each group). (J) BGP-15 improved learning ability in TauKQ mice shown by shortened latency to find the hidden platform during training stage in the MMW test (n = 8–12 mice each group). (K) Representative swimming path of mice in each group during the MWM probe test. (L–O) BGP-15 improved memory ability of TauKQ mice shown as the decreased latency to reach the location of platform placed before (L), the increased crosses in the previous platform area (M) and the increased time stayed in the target quadrant (N) during the MWM probe test. No significant difference in swimming speed among the four groups during the MWM probe test (O) (n = 8–12 mice each group). (P, Q) In FC test, BGP-15 improved fear memory in TauKQ mice shown by increased freezing time at second day (n = 8–12 mice each group).

All data were presented as mean ± SEM. Two-way repeated measures ANOVA test followed by Tukey's post hoc test for B and J, and One-way ANOVA test followed by Tukey's post hoc test for others. B and J: *, $p < 0.05$, **, $p < 0.01$, ****, $p < 0.0001$, vs Vec; &, $p < 0.05$, &&, $p < 0.01$, &&&&, $p < 0.0001$, vs TauKQ. Others: *, $p < 0.05$, **, $p < 0.01$, ***, $p < 0.001$, ****, $p < 0.0001$.

fusion and fission, a process that is essential for maintaining a healthy pool of mitochondria [69]. The unbalance of fusion and fission in mitochondria leads to functional changes, including increased lipid peroxidation, increased production of reactive oxygen species (ROS), decreased membrane potential, respiration and ATP production [70]. The mitochondrial dynamics disorder widely found in the AD brain and animal models [71], Aβ and tau had quite different effects, Aβ induced mitochondria fission [72,73], while total length human tau441 accumulation promoted mitochondria fusion [30]. Here, TauWT increased fusion proteins Mfn1, Mfn2 and OPA1 levels and thus enhancing mitochondrial fusion, shown by increased mitochondria length, which was consistent with our previous study [30]. However, it was surprising to find that, compared with TauWT, TauKQ did not enhance mitochondria fusion, on the contrary, TauKQ induced mitochondria fission. TauKR reversed mitochondria length with increased mitofusion protein compared with those of TauKQ. We have found that wild type tau may span on the outer mitochondrial membrane with some domains exposing to the inter-membrane spaces. The reason for this difference in mitochondrial dynamics may come from the modification of the conformation of tau conducted by the acetylation of the K274/281 sites, which needs further study. In addition to promoting mitochondrial fusion, Mfn1 and Opa1 are also essential for the maintenance of the integrity and density of mitochondrial cristae [74]. In TauKQ-expressing mice, we detected a decrease in Mfn1 and Opa1, which may explain the observed severe loss of mitochondrial cristae and mitochondrial vacuolation under electron microscope. Over-divided mitochondria are supposed to be cleared by mitophagy [64], however, while TauKQ overexpressing, mitophagy was also impaired, the accumulation of dysfunctional mitochondria forms a vicious cycle that may exacerbates the pathology of TauKQ group. The mechanism by which acetylated tau leads to alteration of mitochondrial biogenesis and dynamic homeostasis is not yet known, and remains to be investigated.

Tau acetylated at K274/281 inhibited mitochondrial biogenesis and mitophagy, and induced mitochondrial fission, while non-acetylated at K274/281 induced mitochondrial fusion and inhibited mitophagy, which was as similar as tau441. Tau acetylation specifically increased neuron cell death in an in vitro model of TBI, as indicated by increased cleavage of caspase 3 [75], which was also confirmed in our TauKQ model. Upon damage, the mitochondria release apoptotic proteins such as cytochrome *c* and apoptosis inducible factor (AIF) into the cytosol [76]. Cyt *c* binds with apoptotic protein-activating factor-1 (Apaf-1) and procaspase-9 to form an "apoptosome", which actives caspase-9 and subsequently caspase-3. The cleaved-caspase-3 protein, an important executioner of the apoptotic pathway, is disrupting broad homeostasis and leading to neuronal apoptosis [77]. We also found that TauKQ induced cleaved-caspase-3 level highest, which was consistent with the least neuron number. These data suggested that TauKQ is the most toxic

in three tau forms, which was confirmed by the more severe decreased ATP production and increased ROS level, dendritic plasticity damage, more neuron loss and cognitive deficits.

The disruption of mitochondrial function is considered to be a key cause of the pathophysiology of many neurological diseases, including AD, and the induction or improvement of mitochondrial function by promoting mitochondrial biogenesis, or administration of antioxidants, etc., is considered as a novel therapeutic target and confirmed a modern neuroprotective approach for most of diseases such as neurodegenerative diseases including AD, PD, HD, and ALS in the near future [78–82]. In this study, we applied BGP-15 in TauKQ mice, and observed BGP-15 treatment ameliorated TauKQ-induced neuronal loss and reduced dendritic spines by promoting mitochondrial biogenesis, improving mitochondrial dynamic homeostasis, and protecting mitochondrial function, thereby improving learning and memory capacity in mice. Our experiments demonstrated the potential utility of BGP-15 in a neurological disease model. BGP-15 has been shown to improve metabolic function in several animal models of human degenerative diseases [43,47,48,51,52, 58] and has been administered to more than 400 patients in human clinical trials without serious drug-related adverse events [83]. The data reported here suggests that this drug or a similar compound may exert a protective effect on neurons in AD patients.

4. Limitation

Though recombinant KQ mutant (lysine residues are substituted with glutamine as a mimic of acetyl lysine), and KR mutant (lysine residues are substituted with arginine as a mimic of nonacetylated lysine), are widely used to study the effects of acetylation, there are some limitations. Firstly, using mutant expression is that 100% of the tau protein pool will be acetylated or non-acetylated at those Lys residues. This is neither physiological nor appropriate when considering the dynamic regulation of PTMs such as lysine acetylation. Secondly, it is possible that the effects of in vivo acetylation may be overestimated when the KQ mutant is used as a mimic of the acetylated lysine. For example, acetylation of the lysine residues in the Ku70 ring did not remarkably reduce the affinity of Ku for DNA by the computational approach, although those residues have been acetylated in the in vivo studies [84,85].

5. Materials and methods

5.1. Plasmids, viruses and antibodies

AAV-hSyn-EGFP-MCS-3flag (empty vector, namely AAV-Vec), AAV-hSyn-EGFP-tau-wild-type-3flag (namely AAV-TauWT), AAV-hSyn-EGFP-tau (K274 and K281 mutated to Glutamine)-3flag (namely AAV-TauKQ) and AAV-hSyn-EGFP-tau (K274 and K281 mutated to

Arginine)-3flag (namely AAV-TauKR) were purchased from OBIO Technology (Shanghai, China). The lenti viruses, lenti-hSyn-MCS-EGFP-3flag (empty vector, namely lenti-Vec), lenti-hSyn-tau-wild-type-EGFP-3flag (namely lenti-TauWT), lenti-hSyn-tau (K274 and K281 mutated to Gln)-EGFP-3flag (namely lenti-TauKQ) and lenti-hSyn-tau (K274 and K281 mutated to Arg)-EGFP-3flag (namely lenti-TauKR) were also purchased from OBIO Technology (Shanghai, China). The antibodies used in present study were listed in Supplementary Table 1.

5.2. Primary hippocampal neuron culture

The hippocampus of rat embryos (E17) was dissected and lightly chopped in Hank's buffered saline solution, suspended for 15 min at 37 °C in 0.25% (vol/vol) trypsin solution, and seeded at 30,000–40,000 cells per well on 6-well plates coated with Poly-D-Lysine/Laminin (P7405, Sigma-Aldrich) in neurobasal medium (21,103,049, Thermo-Fisher Scientific) supplemented with 2% B27 (17,504,044, Thermo-Fisher Scientific)/0.5 mM glutamine/25 mM glutamate.

5.3. Animals and stereotactic brain injection

Wild-type C57BL/6 mice (2-month-old, male) were purchased from Beijing Shulaibao Company in accordance with the law of the People's Republic of China on Animal and Plant Inspection and Quarantine. Animals were managed in strict accordance with China's regulations on the Management of experimental animals. Mice were kept in the same environment with a controlled temperature of 23 °C, adequate water, free intake, and a circadian rhythm of 12:12 h. All animal experiments were conducted in accordance with the policy for the use of animals and humans in neuroscience research, and the Institutional Animal Care and Use Committee in Tongji Medical College, Huazhong University of Science and Technology approved the study protocol.

The mice were anesthetized by isoflurane and injected with the viruses (KOPF brain stereotactic locator, Germany). The coordinates for the injection were as follows: CA1 (anterior-posterior: −1.9 mm; mediolateral: −1.2 mm; dorsoventral: ±1.3 mm from bregma and dura, flat skull). Behavioral tests were performed one month after injection, and the mice were then sacrificed for biochemical tests.

5.4. Drug administration

For animals: 20 d after virus injection, mice were treated with BGP-15 ((O-[3-piperidino-2-hydroxy-1-propyl]-nicotinic amidoxime), HY-100828, MCE) at 28 mg/kg body weight or vehicle (physiological saline) daily by gavage for 10 d [51,57].

For primary hippocampal neurons: At 2 div (days in vitro), the primary hippocampal neurons were transfected with lentivirus, given 10 μM BGP-15 separately at 3 div for 5 d [56], half the culture medium was changed every other day until sample collection at 8 div. All cultures were kept at 37 °C in a humidified 5% CO_2 containing atmosphere.

5.5. Novel object recognition (NOR) test

The novel object recognition (NOR) test is a learning and memory assessment method that is based on the principle that animals have an innate tendency to explore new objects. On the first day, mice were placed in the box (50 × 50 × 50 cm) with two identical objects for a 5 min habituation. One of the objects was changed after 24 h and the mouse freely moved around. When the mice were within 3 cm of the object, the experimenter recorded the mice's exploration preference for the object within 5 min. A video camera above the arenas logged the experimental behavior. Before each mouse performed each behavioral experiment, the test bench was sprayed with 75% alcohol and wiped it clean. The novel object preference calculated by new object exploration time/(new object exploration time + old object exploration time) × 100%.

5.6. Morris water maze test

Morris water maze (MWM) test was carried out as described in a previous study [86]. For spatial learning, the mice were trained in a circular pool. The pool is artificially divided into four quadrants. The mice were acclimated for five days before the test. The training time was fixed at 12:00 p.m.-18:00 p.m. In each training session, the mouse was gently placed into a pool with facing the pool wall and allowed to swim freely. The time of the mouse taking to find the platform was recorded as a latency time and the animal allowed to stay on the platform for another 30 s. If the mouse did not find the platform within 60 s, the experimenter gently guided the mouse to the platform and let the mouse stay on the platform for 30 s. Training experiments were conducted three times a day, continued for five days. At 48 h after day 5th, spatial memory was tested by removing the platform. The time the mice reached the position where previous platform placed, the number of times crossed the platform, and the time stayed in the target quadrant were recorded. The motion trails of mice were recorded and analyzed using MWZ-100 system (Techman, China).

5.7. Fear conditioning (FC) test

A box measuring 20 × 20 × 40 cm was equipped with a ceiling-mounted video tracking camera, a light, a speaker, a soundproof door and an electric shock floor. On the first day, put the mouse into the cage to acclimate for 3 min, followed by 3 tone-shock pairings and a 2 s, 0.9 mA foot shock, with an interval of 1 min. The box was cleaned with 75% alcohol to eliminate residual odor. 24 h after the training, the fear memory was tested by subjecting back into the conditioning chamber for 3 min and measuring the freezing time.

5.8. Immunofluorescence

For tissues: The mice were anesthetized with isoflurane. After 0.9% normal saline for blood flushing and 4% paraformaldehyde fixation, the brain was removed and fixed in 4% paraformaldehyde for another 24 h. The brains were dehydrated in 30% sucrose-PBS for 48 h, and then cut into 30 μm. The immunofluorescence (IF) experiments were conducted according to the established method [87]. The slices were incubated with primary antibody. The images were taken using a confocal microscope for IF (Carl Zeiss LSM780).

For primary cultured neurons: After primary neurons infected with the indicated lentivirus, they were fixed with 4% paraformaldehyde for 15 min, permeabilized with 0.1% Triton X-100 for 30 min, and blocked with 5% bovine serum albumin for another 30 min, then immunostained using primary antibodies for 1 h at room temperature. Followed by washing, fluorescent dye-conjugated secondary antibodies were incubated for 1 h at room temperature. All mounted samples were examined and imaged on a confocal microscope LSM780 equipped with a 63× oil immersion objective (Carl Zeiss). For Sholl analysis, at least 15 primary hippocampal neurons were used for each group by Fiji software [88].

5.9. Protein extraction and western blotting

The hippocampus was separated from the mouse brain. Hippocampal regions infected with virus were isolated, and homogenized in lysis buffer for Western blotting (P0013, Beyotime). Homogenate was mixed with 8% (wt/vol) SDS buffer, boiled at 95 °C for 10 min, and decomposed by ultrasonic.

Western blotting (WB) was performed according to the method established in our laboratory [89]. The sample was loaded according to the concentration and performed SDS-polyacrylamide gel electrophoresis separation. After the separation, the gel was transferred to the nitrocellulose (NC) membrane. After that, the NC membrane was blocked with 5% skim milk for 1 h and incubated with the primary antibody overnight at 4 °C, then washed with TBS-Tween20 (TBST) and

incubated with the Odyssey secondary antibody for 1 h at room temperature, washed again with TBST and imaged by Odyssey (LI-COR Biosciences, USA), finally quantitatively analyzed by ImageJ software.

5.10. Immunoprecipitation (IP)

The hippocampal CA1 tissues were homogenized on ice in RIPA buffer (P0013D, Beyotime) and then centrifuged at 12,000×g for 20 min. A total of 200 μl supernatants containing approximately 200 μg of total proteins were incubated with primary antibodies (Table S1) overnight, followed by addition of protein G agarose (IP05, Millipore) for 6h (rotating at 4 °C). The agarose beads were washed three times and resuspended in 40 μl of SDS-loading buffer, and then denatured at 95 °C for 10 min. The immunoprecipitants were analyzed by Western blotting.

5.11. Nissl's staining

Mouse brain sections (frozen sections, 30 μm thick) were washed with PBS for 3 × 5 min, and then dyed with 0.5% toluidine blue reagent (G1036, Servicebio) for 5 min, then slices were dehydrated through graded ethanol (75%, 85%, 90%, 100%, 100%) for 10 min each time, transparentized in xylene for 30 min, then slices were mounted with neutral balsam and imaged by a scanning microscope (SV120, OLYMPUS).

5.12. Relative mitochondrial copy number

The relative mitochondrial DNA (mtDNA) copy number, which expressed as mtDNA/nDNA (nuclear DNA), was measured by qPCR. Total DNA was extracted using the QIAamp DNA Mini Kit (51304, Qiagen) and operated according to previous research [90]. The primers of mitochondrial DNA: (F) GCCAGCCTGACCCATAGCCATAAT and (R) GCCGGCTGCGTATTCTACGTTA. And the primers of nuclear control: (F) TTGAGACTGTGATTGGCAATGCCT and (R) CCAGAAATGCTGGGCGTACT.

5.13. Mitochondrial functional assays

ATP assay: We used an ATP Assay Kit (S0026, Beyotime) to detect ATP levels in hippocampal CA1 tissues. Briefly, the hippocampal regions infected with virus was extracted and lysed with an ATP lysis buffer. After protein extraction and measurement, the reaction mixture contained sample protein or standard (100 μl) with ATP detection fluid (100 μl) was incubated at room temperature for 3–5 min. The luminescence was measured using a microplate reader. ATP levels were calculated according to the standard curve and presented as nmol/mg protein.

SOD activity assay: The SOD Assay Kit were used for evaluation SOD activity (S0103, Beyotime) in hippocampal CA1 tissues according to the manufacturer's instructions. The absorbance was assessed at 450 nm using a microplate reader, SOD activity was normalized to the total protein.

Intracellular ROS assay: We used 2′,7′-Dichlorodihydrofluorescein diacetate (DCFH-DA) (S0033, Beyotime) as a probe to detect intracellular ROS levels. Briefly, the primary hippocampal neurons were seeded at 30,000–40,000 cells per well on 6-well plates, transfected with lentivirus at 2 div, and at 8 div, neurons were stained with DCFH-DA in serum and phenol red-free medium for 30 min at 37 °C in a humidified incubator with 5% CO_2/95% air (v/v) at 37 °C. Neurons were washed three times with sterile PBS and then observed under a fluorescent microscope (Nikon, Ti–S, Japan).

Mitochondrial ROS assay: The mitochondrial ROS production was monitored using MitoSox Red probe (40778ES50, Yeasen). Briefly, the primary hippocampal neurons were seeded at 30,000–40,000 cells per well on 6-well plates, transfected with lentivirus at 2 div, and at 8 div, neurons were cultured with serum-free culture medium containing 5 μM

MitoSox Red probe for 10 min at 37 °C. After that, the neurons were washed 3 times with warm PBS to remove excess dye and observed under a fluorescent microscope (Nikon, Ti–S, Japan).

Measurement of mitochondrial membrane potential (MMP): TMRE kits (Mitochondrial Membrane Potential Assay Kit with TMRE) (C2001, Beyotime) were used to assess the MMP level of cells according to the manufacture's protocols. Briefly, primary hippocampal neurons were seeded at 30,000–40,000 cells per well on 6-well plates, transfected with lentivirus at 2 div, and at 8 div, TMRE (tetramethylrhodamine, ethyl ester) staining solution was added to the neurons, incubated for 30 min at 37 °C. After washed twice with staining buffer, the neurons were observed under a fluorescent microscope (Nikon, Ti–S, Japan).

5.14. Measurement of mitochondrial length

In primary hippocampal neurons, mitochondria were labeled with MitoTracker™ Red CMXRos (M7512, Invitrogen™) according to the manufacturer's protocol, and nuclei were labeled with DAPI (C1002, Beyotime). The mitochondria imaged by confocal microscopy (Zeiss LSM780 laser scanning confocal microscope, 63 × /1.46 objective) with the ZEN program. Neuronal process 100–200 μM from the body were used for measuring average mitochondrial length by using ImageJ software.

5.15. Transmission electron microscopy

Mice were anesthetized and brains were removed and stored overnight in 2.5% glutaraldehyde. The next day, the brains were sliced into 50 mm thick slices using a vibrating knife. The CA1 region of the mouse hippocampus was taken and post-treated in 1% Cesium tetroxide solution for 1 h, dehydrated in graded ethanol and epoxy resin-embedded. The polymerization reaction was carried out at 80 °C for 24 h. The sections (60–70 nm) stained with uranyl acetate and lead citrate, and observed under a Hitachi 7100 electron microscope (Nikon, Tokyo, Japan). For the quantification of mitochondrial morphology, we referred to a published study in which mitochondrial morphology was divided into four categories based on the value of mitochondrial length/diameter (L/D), and mitochondria were divided into three categories based on cristae morphology [91]. At least 100 mitochondria from three mice per group were analyzed, the proportion of each type of mitochondria in each group was shown.

5.16. Golgi staining

Golgi staining was performed by using a FD Rapid GolgiStain Kit (PK401, FD Neurotechnology) according to the manufacturer's instructions. The mice were anesthetized and their brains were immersed in a mixture of AB (1:1) solution. After 24 h, the brain tissue was replaced with the new AB solution and soaked for 1 month. The brain tissue was soaked in C solution for 3–7 d, after which it was placed on an oscillating tissue slicer and cut into slices (100 μm thick). After being air dried in the dark, the slices were rinsed in ddH₂O for 2 × 4 min, stained with a mixture of solution D + E + double distilled water (1:1:2) for 10 min, and rinsed in ddH₂O for 2 × 4 min. Slices were dehydrated through graded ethanol (50%, 75%, 95%) for 4 min each time, and anhydrous ethanol for 4 × 4 min, and followed with transparentizing in xylene for 30 min. Images were taken using an optical microscope (Nikon, Japan).

5.17. Reverse transcription and real-time quantitative PCR

Reverse transcription and real-time quantitative PCR were carried out as established in our laboratory [37]. The PCR system consisted of 3 mM $MgCl_2$, 0.5 μM forward and reverse primers, 2 μl SYBR Green PCR master mixes, and 2 μl cDNA, and the standards for each gene were prepared using appropriate primers by a conventional PCR. The samples were assayed on a Rotor-Gene 300 Real-time Cycler (Corbett Research,

Sydney, Australia). The expression level of the gene was normalized by the housekeeping gene GAPDH, which was not affected by the treatment. PCR primers employed in the present study are as follows: Mfn1 forward and reverse primers, 5′-GCAGACAGCACATGGAGAGA-3′ and 5′-GATCCGATTCCGAGCTTCCG-3′; Mfn2 forward and reverse primers, 5′-TGCACCGCCATATAGAGGAAG-3′ and 5′-TCTGCAGTGAACTGG-CAATG-3′; Opa1 forward and reverse primers, 5′-ACCTTGCCAGTTTAGCTCCC-3′ and 5′-TTGGGACCTGCAGTGAA-GAA-3′; Drp1 forward and reverse primers, 5′-ATGCCAGCAAGTCCACAGAA-3′ and 5′-TGTTCTCGGGCAGA-CAGTTT-3′; Fis1 forward and reverse primers, 5′-CAAAGAGGAACAGCGGGACT-3′ and 5′-ACAGCCCTCGCACA-TACTTT-3′; PGC1-α forward and reverse primers, 5′-GCAGTCGCAACATGCTCAAG-3′ and 5′-GGGAACCCTTGGGGT-CATTT-3′; Nrf1 forward and reverse primers, 5′-AGAAACGGAAACGGCCTCAT-3′ and 5′-CATCCAACGTGGCTCT-GAGT -3′; and Tfam forward and reverse primers, 5′- TCCACAGAA-CAGCTACCCAA -3′ and 5′-AGACGGTTGTTGATTAGGCGT-3′ and GAPDH forward and reverse primers, 5′-TTCCCGTTCAGCTCTGGG-3′ and 5′-CCCTGCATCCACTGGTGC-3′.

5.18. Statistical analyses

The data were presented as mean ± SEM, and analyzed using GraphPad Prism (GraphPad Software, Inc., La Jolla, CA, United States). Statistical analyses were conducted using one-way ANOVA or two-way ANOVA followed by Tukey multiple-comparisons post hoc tests. The statistically significance was set at $P < 0.05$. According to the article method [92,93], we estimated the sample size using pre-experimental data, the required sample size was calculated by G*power, effect size = 1.264, α = 0.05, Power = 0.8, Number of groups = 4, and the calculated sample size of each group is n = 3.

Data and material availability statement

Animal care was carried out following the provision and general recommendation of the Chinese Experimental Animals Administration Legislation. The procedure was approved by the Animal Protection and Use Committee of Huazhong University of Science & Technology. This manuscript does not contain patient data or clinical studies. The data used to support the findings of this study are available from the corresponding author upon request.

Author contribution

G.P.L, Z.J.Z, and G.P. W designed the experiments. Q.L, X.W and C. H. H performed all animal behavioral tests. Q.L performed mitochondrial functional assays and Golgi staining. X.W performed IHC and IF. Q. L, X.W, Y.H, J.N.Z performed Western blotting. T.L, B.G.Z, Y.H and Y. Q. W analyzed the data. G.P.L wrote the manuscript. All authors read and approved the final manuscript.

Funding

Declaration of competing interest

We all authors stated that we have no conflicts of interest. Qian Liu, Xin Wang, Yu Hu, Jun-Ning Zhao, Chun-Hui Huang, Ting Li, Bing-Ge Zhang, Ye He, Yan-Qing Wu, Zai-Jun Zhang, Guo-Ping Wang, Gong-Ping Liu.

Data availability

Data will be made available on request.

Appendix A. Supplementary data

Supplementary data to this article can be found online at https://doi.org/10.1016/j.redox.2023.102697.

References

[1] S. Epelbaum, R. Genthon, E. Cavedo, M.O. Habert, F. Lamari, G. Gagliardi, S. Lista, M. Teichmann, H. Bakardjian, H. Hampel, B. Dubois, Preclinical Alzheimer's disease: a systematic review of the cohorts underlying the concept, Alzheimers Dement. 13 (2017) 454–467.

[2] D.M. Holtzman, M.C. Carrillo, J.A. Hendrix, L.J. Bain, A.M. Catafau, L.M. Gault, M. Goedert, E. Mandelkow, E.M. Mandelkow, D.S. Miller, S. Ostrowitzki, M. Polydoro, S. Smith, M. Wittmann, Hutton M. Tau, From research to clinical development, Alzheimers Dement. 12 (2016) 1033–1039.

[3] W. Mair, J. Muntel, K. Tepper, S. Tang, J. Biernat, W.W. Seeley, K.S. Kosik, E. Mandelkow, H. Steen, J.A. Steen, FLEXITau: quantifying post-translational modifications of tau protein in vitro and in human disease, Anal. Chem. 88 (2016) 3704–3714.

[4] J. Zheng, N. Tian, F. Liu, Y. Zhang, J. Su, Y. Gao, M. Deng, L. Wei, J. Ye, H. Li, J. Z. Wang, A novel dephosphorylation targeting chimera selectively promoting tau removal in tauopathies, Signal Transduct. Targeted Ther. 6 (2021) 269.

[5] J. Zheng, H.L. Li, N. Tian, F. Liu, L. Wang, Y. Yin, L. Yue, L. Ma, Y. Wan, J.Z. Wang, Interneuron accumulation of phosphorylated tau impairs adult hippocampal neurogenesis by suppressing GABAergic transmission, Cell Stem Cell 26 (2020) 331–345 e336.

[6] J.Z. Wang, Y.Y. Xia, I. Grundke-Iqbal, K. Iqbal, Abnormal hyperphosphorylation of tau: sites, regulation, and molecular mechanism of neurofibrillary degeneration, J. Alzheimers Dis. 33 (Suppl 1) (2013) S123–S139.

[7] J.Z. Wang, Z.H. Wang, Tian, Q Tau hyperphosphorylation induces apoptotic escape and triggers neurodegeneration in Alzheimer's disease, Neurosci. Bull. 30 (2014) 359–366.

[8] T.E. Tracy, Gan L Acetylated tau in Alzheimer's disease: an instigator of synaptic dysfunction underlying memory loss: increased levels of acetylated tau blocks the postsynaptic signaling required for plasticity and promotes memory deficits associated with tauopathy, Bioessays 39 (2017).

[9] T.E. Tracy, P.D. Sohn, S.S. Minami, C. Wang, S.W. Min, Y. Li, Y. Zhou, D. Le, I. Lo, R. Ponnusamy, X. Cong, B. Schilling, L.M. Ellerby, R.L. Huganir, L. Gan, Acetylated tau obstructs KIBRA-mediated signaling in synaptic plasticity and promotes tauopathy-related memory loss, Neuron 90 (2016) 245–260.

[10] D.J. Irwin, T.J. Cohen, M. Grossman, S.E. Arnold, S.X. Xie, V.M.Y. Lee, Trojanowski JQ Acetylated tau, a novel pathological signature in Alzheimer's disease and other tauopathies, Brain 135 (2012) 807–818.

[11] S.W. Min, S.H. Cho, Y. Zhou, S. Schroeder, V. Haroutunian, W.W. Seeley, E. J. Huang, Y. Shen, E. Masliah, C. Mukherjee, D. Meyers, P.A. Cole, M. Ott, L. Gan, Acetylation of tau inhibits its degradation and contributes to tauopathy, Neuron 67 (2010) 953–966.

[12] T. Arakhamia, C.E. Lee, Y. Carlomagno, M. Kumar, D.M. Duong, M. Wesseling, S. R. Kundinger, K. Wang, D. Williams, M. DeTure, D.W. Dickson, C.N. Cook, N. T. Seyfried, L. Petrucelli, J.A. Steen, Fitzpatrick AWP posttranslational modifications mediate the structural diversity of tauopathy strains, Cell 184 (2021) 6207–6210.

[13] M. Morris, G.M. Knudsen, S. Maeda, J.C. Trinidad, A. Ioanoviciu, A.L. Burlingame, Mucke L Tau post-translational modifications in wild-type and human amyloid precursor protein transgenic mice, Nat. Neurosci. 18 (2015) 1183–1189.

[14] H.B. Luo, Y.Y. Xia, X.J. Shu, Z.C. Liu, Y. Feng, X.H. Liu, G. Yu, G. Yin, Y.S. Xiong, K. Zeng, J. Jiang, K.Q. Ye, X.C. Wang, J.Z. Wang, SUMOylation at K340 inhibits tau degradation through deregulating its phosphorylation and ubiquitination, Proc. Natl. Acad. Sci. U. S. A. 111 (2014) 16586–16591.

[15] C.X. Gong, F. Liu, K. Iqbal, O-GlcNAcylation: a regulator of tau pathology and neurodegeneration, Alzheimers Dement. 12 (2016) 1078–1089.

[16] J.Z. Wang, I. Grundke-Iqbal, K. Iqbal, Glycosylation of microtubule-associated protein tau: an abnormal posttranslational modification in Alzheimer's disease, Nat. Med. 2 (1996) 871–875.

[17] S.W. Min, X. Chen, T.E. Tracy, Y. Li, Y. Zhou, C. Wang, K. Shirakawa, S.S. Minami, E. Defensor, S.A. Mok, P.D. Sohn, B. Schilling, X. Cong, L. Ellerby, B.W. Gibson, J. Johnson, N. Krogan, M. Shamloo, J. Gestwicki, E. Masliah, E. Verdin, L. Gan, Critical role of acetylation in tau-mediated neurodegeneration and cognitive deficits, Nat. Med. 21 (2015) 1154–1162.

[18] T.J. Cohen, J.L. Guo, D.E. Hurtado, L.K. Kwong, I.P. Mills, J.Q. Trojanowski, V. M. Lee, The acetylation of tau inhibits its function and promotes pathological tau aggregation, Nat. Commun. 2 (2011) 252.

[19] M. Golpich, E. Amini, F. Hemmati, N.M. Ibrahim, B. Rahmani, Z. Mohamed, A. A. Raymond, L. Dargahi, R. Ghasemi, Ahmadiani A Glycogen synthase kinase-3 beta (GSK-3beta) signaling: implications for Parkinson's disease, Pharmacol. Res. 97 (2015) 16–26.

[20] H. Chen, Chan DC Mitochondrial dynamics–fusion, fission, movement, and mitophagy–in neurodegenerative diseases, Hum. Mol. Genet. 18 (2009) R169–R176.

[21] R. McFarland, R.W. Taylor, D.M. Turnbull, A neurological perspective on mitochondrial disease, Lancet Neurol. 9 (2010) 829–840.

[22] M.T. Lin, Beal MF Mitochondrial dysfunction and oxidative stress in neurodegenerative diseases, Nature 443 (2006) 787–795.

[23] J. Yao, R.W. Irwin, L. Zhao, J. Nilsen, R.T. Hamilton, Brinton RD Mitochondrial bioenergetic deficit precedes Alzheimer's pathology in female mouse model of Alzheimer's disease, Proc. Natl. Acad. Sci. U. S. A. 106 (2009) 14670–14675.

[24] J. Neustadt, Pieczenik SR Medication-induced mitochondrial damage and disease, Mol. Nutr. Food Res. 52 (2008) 780–788.

[25] B. Sheng, X. Wang, B. Su, H.G. Lee, G. Casadesus, G. Perry, Zhu, X Impaired mitochondrial biogenesis contributes to mitochondrial dysfunction in Alzheimer's disease, J. Neurochem. 120 (2012) 419–429.

[26] D.F. Suen, K.L. Norris, Youle RJ Mitochondrial dynamics and apoptosis, Genes Dev. 22 (2008) 1577–1590.

[27] M. Manczak, Reddy PH Abnormal interaction between the mitochondrial fission protein Drp1 and hyperphosphorylated tau in Alzheimer's disease neurons: implications for mitochondrial dysfunction and neuronal damage, Hum. Mol. Genet. 21 (2012) 2538–2547.

[28] R.A. Quintanilla, T.A. Matthews-Roberson, P.J. Dolan, Johnson GV Caspase-cleaved tau expression induces mitochondrial dysfunction in immortalized cortical neurons: implications for the pathogenesis of Alzheimer disease, J. Biol. Chem. 284 (2009) 18754–18766.

[29] R.A. Quintanilla, R. von Bernhardi, J.A. Godoy, N.C. Inestrosa, Johnson GV Phosphorylated tau potentiates Abeta-induced mitochondrial damage in mature neurons, Neurobiol. Dis. 71 (2014) 260–269.

[30] X.C. Li, Y. Hu, Z.H. Wang, Y. Luo, Y. Zhang, X.P. Liu, Q. Feng, Q. Wang, K. Ye, G. P. Liu, J.Z. Wang, Human wild-type full-length tau accumulation disrupts mitochondrial dynamics and the functions via increasing mitofusins, Sci. Rep. 6 (2016), 24756.

[31] M.K. Gorsky, S. Burnouf, O. Sofola-Adesakin, J. Dols, H. Augustin, C.M. Weigelt, S. Gronke, L. Partridge, Pseudo-acetylation of multiple sites on human Tau proteins alters Tau phosphorylation and microtubule binding, and ameliorates amyloid beta toxicity, Sci. Rep. 7 (2017) 9984.

[32] H. Wesseling, W. Mair, M. Kumar, C.N. Schlaffner, S. Tang, P. Beerepoot, B. Fatou, A.J. Guise, L. Cheng, S. Takeda, J. Muntel, M.S. Rotunno, S. Dujardin, P. Davies, K. S. Kosik, B.L. Miller, S. Berretta, J.C. Hedreen, L.T. Grinberg, W.W. Seeley, B. T. Hyman, H. Steen, Steen JA tau PTM profiles identify patient heterogeneity and stages of alzheimer's disease, Cell 183 (2020) 1699–1713 e1613.

[33] A. Bejanin, D.R. Schonhaut, R. La Joie, J.H. Kramer, S.L. Baker, N. Sosa, N. Ayakta, A. Cantwell, M. Janabi, M. Lauriola, J.P. O'Neil, M.L. Gorno-Tempini, Z.A. Miller, H.J. Rosen, B.L. Miller, W.J. Jagust, Rabinovici GD Tau pathology and neurodegeneration contribute to cognitive impairment in Alzheimer's disease, Brain 140 (2017) 3286–3300.

[34] Y. Tatebayashi, M.H. Lee, L. Li, K. Iqbal, Grundke-Iqbal I the dentate gyrus neurogenesis: a therapeutic target for Alzheimer's disease, Acta Neuropathol. 105 (2003) 225–232.

[35] P. Giannakopoulos, F.R. Herrmann, T. Bussiere, C. Bouras, E. Kovari, D.P. Perl, J. H. Morrison, G. Gold, P.R. Hof, Tangle and neuron numbers, but not amyloid load, predict cognitive status in Alzheimer's disease, Neurology 60 (2003) 1495–1500.

[36] Y. Yin, D. Gao, Y. Wang, Z.H. Wang, X. Wang, J. Ye, D. Wu, L. Fang, G. Pi, Y. Yang, X.C. Wang, C. Lu, K. Ye, J.Z. Wang, Tau accumulation induces synaptic impairment and memory deficit by calcineurin-mediated inactivation of nuclear CaMKIV/CREB signaling, Proc. Natl. Acad. Sci. U. S. A. 113 (2016) E3773–E3781.

[37] X.G. Li, X.Y. Hong, Y.L. Wang, S.J. Zhang, J.F. Zhang, X.C. Li, Y.C. Liu, D.S. Sun, Q. Feng, J.W. Ye, Y. Gao, D. Ke, Q. Wang, H.L. Li, K. Ye, G.P. Liu, J.Z. Wang, Tau accumulation triggers STAT1-dependent memory deficits by suppressing NMDA receptor expression, EMBO Rep. 20 (2019).

[38] M. Golpich, B. Rahmani, N. Mohamed Ibrahim, L. Dargahi, Z. Mohamed, A. A. Raymond, Ahmadiani A Preconditioning as a potential strategy for the prevention of Parkinson's disease, Mol. Neurobiol. 51 (2015) 313–330.

[39] Q. Feng, Y. Luo, X.N. Zhang, X.F. Yang, X.Y. Hong, D.S. Sun, X.C. Li, Y. Hu, X.G. Li, J.F. Zhang, X. Li, Y. Yang, Q. Wang, G.P. Liu, J.Z. Wang, MAPT/Tau accumulation represses autophagy flux by disrupting IST1-regulated ESCRT-III complex formation: a vicious cycle in Alzheimer neurodegeneration, Autophagy 16 (2020) 641–658.

[40] L. Tilokani, S. Nagashima, V. Paupe, Prudent J Mitochondrial dynamics: overview of molecular mechanisms, Essays Biochem. 62 (2018) 341–360.

[41] Y. Zhang, X. Liu, J. Bai, X. Tian, X. Zhao, W. Liu, X. Duan, W. Shang, H.Y. Fan, Tong C mitoguardin regulates mitochondrial fusion through MitoPLD and is required for neuronal homeostasis, Mol. Cell 61 (2016) 111–124.

[42] E. Szabados, P. Literati-Nagy, B. Farkas, Sumegi B BGP-15, a nicotinic amidoxime derivate protecting heart from ischemia reperfusion injury through modulation of poly(ADP-ribose) polymerase, Biochem. Pharmacol. 59 (2000) 937–945.

[43] R. Halmosi, Z. Berente, E. Osz, K. Toth, P. Literati-Nagy, Sumegi B Effect of poly (ADP-ribose) polymerase inhibitors on the ischemia-reperfusion-induced oxidative cell damage and mitochondrial metabolism in Langendorff heart perfusion system, Mol. Pharmacol. 59 (2001) 1497–1505.

[44] I. Racz, K. Tory, F. Gallyas Jr., Z. Berente, E. Osz, L. Jaszlits, S. Bernath, B. Sumegi, G. Rabloczky, P. Literati-Nagy, BGP-15 - a novel poly(ADP-ribose) polymerase inhibitor - protects against nephrotoxicity of cisplatin without compromising its antitumor activity, Biochem. Pharmacol. 63 (2002) 1099–1111.

[45] G. Bardos, K. Moricz, L. Jaszlits, G. Rabloczky, K. Tory, I. Racz, S. Bernath, B. Sumegi, B. Farkas, B. Literati-Nagy, P. Literati-Nagy, BGP-15, a hydroximic acid derivative, protects against cisplatin- or taxol-induced peripheral neuropathy in rats, Toxicol. Appl. Pharmacol. 190 (2003) 9–16.

[46] J. Chung, A.K. Nguyen, D.C. Henstridge, A.G. Holmes, M.H. Chan, J.L. Mesa, G. I. Lancaster, R.J. Southgate, C.R. Bruce, S.J. Duffy, I. Horvath, R. Mestril, M. J. Watt, P.L. Hooper, B.A. Kingwell, L. Vigh, A. Hevener, Febbraio MA HSP72 protects against obesity-induced insulin resistance, Proc. Natl. Acad. Sci. U. S. A. 105 (2008) 1739–1744.

[47] G. Nagy, A. Szarka, G. Lotz, J. Doczi, L. Wunderlich, A. Kiss, K. Jemnitz, Z. Veres, G. Banhegyi, Z. Schaff, B. Sumegi, Mandl J BGP-15 inhibits caspase-independent programmed cell death in acetaminophen-induced liver injury, Toxicol. Appl. Pharmacol. 243 (2010) 96–103.

[48] Z. Sarszegi, E. Bognar, B. Gaszner, A. Konyi, F. Gallyas Jr., B. Sumegi, Z. Berente, BGP-15, a PARP-inhibitor, prevents imatinib-induced cardiotoxicity by activating Akt and suppressing JNK and p38 MAP kinases, Mol. Cell. Biochem. 365 (2012) 129–137.

[49] S.M. Gehrig, C. van der Poel, T.A. Sayer, J.D. Schertzer, D.C. Henstridge, J. E. Church, S. Lamon, A.P. Russell, K.E. Davies, M.A. Febbraio, G.S. Lynch, Hsp72 preserves muscle function and slows progression of severe muscular dystrophy, Nature 484 (2012) 394–398.

[50] G. Sapra, Y.K. Tham, N. Cemerlang, A. Matsumoto, H. Kiriazis, B.C. Bernardo, D. C. Henstridge, J.Y. Ooi, L. Pretorius, E.J. Boey, L. Lim, J. Sadoshima, P.J. Meikle, N. A. Mellet, E.A. Woodcock, S. Marasco, T. Ueyama, X.J. Du, M.A. Febbraio, J. R. McMullen, The small-molecule BGP-15 protects against heart failure and atrial fibrillation in mice, Nat. Commun. 5 (2014) 5705.

[51] D.C. Henstridge, C.R. Bruce, B.G. Drew, K. Tory, A. Kolonics, E. Estevez, J. Chung, N. Watson, T. Gardner, R.S. Lee-Young, T. Connor, M.J. Watt, K. Carpenter, M. Hargreaves, S.L. McGee, A.L. Hevener, Febbraio MA Activating HSP72 in rodent skeletal muscle increases mitochondrial number and oxidative capacity and decreases insulin resistance, Diabetes 63 (2014) 1881–1894.

[52] L.L. Wu, D.L. Russell, S.L. Wong, M. Chen, T.S. Tsai, J.C. St John, R.J. Norman, M. A. Febbraio, J. Carroll, R.L. Robker, Mitochondrial dysfunction in oocytes of obese mothers: transmission to offspring and reversal by pharmacological endoplasmic reticulum stress inhibitors, Development 142 (2015) 681–691.

[53] H. Salah, M. Li, N. Cacciani, S. Gastaldello, H. Ogilvie, H. Akkad, A.V. Namuduri, V. Morbidoni, K.A. Artemenko, G. Balogh, V. Martinez-Redondo, P. Jannig, Y. Hedstrom, B. Dworkin, J. Bergquist, J. Ruas, L. Vigh, L. Salviati, L. Larsson, The chaperone co-inducer BGP-15 alleviates ventilation-induced diaphragm dysfunction, Sci. Transl. Med. 8 (2016) 350ra103.

[54] T.L. Kennedy, K. Swiderski, K.T. Murphy, S.M. Gehrig, C.L. Curl, C. Chandramouli, M.A. Febbraio, L.M. Delbridge, R. Koopman, G.S. Lynch, BGP-15 improves aspects of the dystrophic pathology in mdx and dko mice with differing efficacies in heart and skeletal muscle, Am. J. Pathol. 186 (2016) 3246–3260.

[55] M.J. Eacott, Gaffan D Reaching to a rewarded visual stimulus: interhemispheric conflict and hand use in monkeys with forebrain commissurotomy, Brain 112 (Pt 5) (1989) 1215–1230.

[56] S.B. Ohlen, M.L. Russell, M.J. Brownstein, Lefcort F BGP-15 prevents the death of neurons in a mouse model of familial dysautonomia, Proc. Natl. Acad. Sci. U. S. A. 114 (2017) 5035–5040.

[57] A. Szabo, K. Sumegi, K. Fekete, E. Hocsak, B. Debreceni, G. Setalo Jr., K. Kovacs, L. Deres, A. Kengyel, D. Kovacs, J. Mandl, M. Nyitrai, M.A. Febbraio, F. Gallyas Jr., Sumegi B Activation of mitochondrial fusion provides a new treatment for mitochondria-related diseases, Biochem. Pharmacol. 150 (2018) 86–96.

[58] O. Horvath, K. Ordog, K. Bruszt, L. Deres, F. Gallyas, B. Sumegi, K. Toth, Halmosi R BGP-15 protects against heart failure by enhanced mitochondrial biogenesis and decreased fibrotic remodelling in spontaneously hypertensive rats, Oxid. Med. Cell. Longev. 2021 (2021), 1250858.

[59] M. Golpich, E. Amini, Z. Mohamed, R. Azman Ali, N. Mohamed Ibrahim, Ahmadiani A mitochondrial dysfunction and biogenesis in neurodegenerative diseases: pathogenesis and treatment, CNS Neurosci. Ther. 23 (2017) 5–22.

[60] D.C. David, S. Hauptmann, I. Scherping, K. Schuessel, U. Keil, P. Rizzu, R. Ravid, S. Drose, U. Brandt, W.E. Muller, A. Eckert, Gotz J Proteomic and functional analyses reveal a mitochondrial dysfunction in P301L tau transgenic mice, J. Biol. Chem. 280 (2005) 23802–23814.

[61] J.S. Kerr, B.A. Adriaanse, N.H. Greig, M.P. Mattson, M.Z. Cader, V.A. Bohr, Fang EF. Mitophagy, Alzheimer's disease: cellular and molecular mechanisms, Trends Neurosci. 40 (2017) 151–166.

[62] M.W. Park, H.W. Cha, J. Kim, J.H. Kim, H. Yang, S. Yoon, N. Boonpraman, S.S. Yi, I.D. Yoo, J.S. Moon, NOX4 promotes ferroptosis of astrocytes by oxidative stress-induced lipid peroxidation via the impairment of mitochondrial metabolism in Alzheimer's diseases, Redox Biol. 41 (2021), 101947.

[63] W. Wang, F. Zhao, X. Ma, G. Perry, X. Zhu, Mitochondria dysfunction in the pathogenesis of Alzheimer's disease: recent advances, Mol. Neurodegener. 15 (2020) 30.

[64] V. Romanello, Sandri M the connection between the dynamic remodeling of the mitochondrial network and the regulation of muscle mass, Cell. Mol. Life Sci. 78 (2021) 1305–1328.

[65] X.J. Jiang, Y.Q. Wu, R. Ma, Y.M. Chang, L.L. Li, J.H. Zhu, G.P. Liu, G. Li, PINK1 alleviates cognitive impairments via attenuating pathological tau aggregation in a mouse model of tauopathy, Front. Cell Dev. Biol. 9 (2021), 736267.

[66] B. Gong, Y. Pan, P. Vempati, W. Zhao, L. Knable, L. Ho, J. Wang, M. Sastre, K. Ono, A.A. Sauve, Pasinetti GM Nicotinamide riboside restores cognition through an upregulation of proliferator-activated receptor-gamma coactivator 1alpha regulated beta-secretase 1 degradation and mitochondrial gene expression in Alzheimer's mouse models, Neurobiol. Aging 34 (2013) 1581–1588.

[67] I.G. Onyango, J. Lu, M. Rodova, E. Lezi, A.B. Crafter, Swerdlow RH Regulation of neuron mitochondrial biogenesis and relevance to brain health, Biochim. Biophys. Acta 1802 (2010) 228–234.

[68] Q. Zhang, J.T. Yu, P. Wang, W. Chen, Z.C. Wu, H. Jiang, L. Tan, Mitochondrial transcription factor A (TFAM) polymorphisms and risk of late-onset Alzheimer's disease in Han Chinese, Brain Res. 1368 (2011) 355–360.

[69] M. Giacomello, A. Pyakurel, C. Glytsou, L. Scorrano, The cell biology of mitochondrial membrane dynamics, Nat. Rev. Mol. Cell Biol. 21 (2020) 204–224.

[70] M.J. Calkins, Reddy PH Assessment of newly synthesized mitochondrial DNA using BrdU labeling in primary neurons from Alzheimer's disease mice: implications for impaired mitochondrial biogenesis and synaptic damage, Biochim. Biophys. Acta 1812 (2011) 1182–1189.

[71] B. DuBoff, M. Feany, J. Gotz, Why size matters - balancing mitochondrial dynamics in Alzheimer's disease, Trends Neurosci. 36 (2013) 325–335.

[72] D.J. Bonda, M.A. Smith, G. Perry, H.G. Lee, X. Wang, X. Zhu, The mitochondrial dynamics of Alzheimer's disease and Parkinson's disease offer important opportunities for therapeutic intervention, Curr. Pharmaceut. Des. 17 (2011) 3374–3380.

[73] L. Zhang, S. Trushin, T.A. Christensen, B.V. Bachmeier, B. Gateno, A. Schroeder, J. Yao, K. Itoh, H. Sesaki, W.W. Poon, K.H. Gylys, E.R. Patterson, J.E. Parisi, R. Diaz Brinton, J.L. Salisbury, E. Trushina, Altered brain energetics induces mitochondrial fission arrest in Alzheimer's Disease, Sci. Rep. 6 (2016), 18725.

[74] S. Cogliati, C. Frezza, M.E. Soriano, T. Varanita, R. Quintana-Cabrera, M. Corrado, S. Cipolat, V. Costa, A. Casarin, L.C. Gomes, E. Perales-Clemente, L. Salviati, P. Fernandez-Silva, J.A. Enriquez, L. Scorrano, Mitochondrial cristae shape determines respiratory chain supercomplexes assembly and respiratory efficiency, Cell 155 (2013) 160–171.

[75] M.K. Shin, E. Vazquez-Rosa, Y. Koh, M. Dhar, K. Chaubey, C.J. Cintron-Perez, S. Barker, E. Miller, K. Franke, M.F. Noterman, D. Seth, R.S. Allen, C.T. Motz, S. R. Rao, L.A. Skelton, M.T. Pardue, S.J. Fliesler, C. Wang, T.E. Tracy, L. Gan, D. J. Liebl, Savarraj Jpj, G.L. Torres, H. Ahnstedt, L.D. McCullough, R.S. Kitagawa, H. A. Choi, P. Zhang, Y. Hou, C.W. Chiang, L. Li, F. Ortiz, J.A. Kilgore, N.S. Williams, V.C. Whitehair, T. Gefen, M.E. Flanagan, J.S. Stamler, M.K. Jain, A. Kraus, F. Cheng, J.D. Reynolds, Pieper AA Reducing acetylated tau is neuroprotective in brain injury, Cell 184 (2021) 2715–2732 e2723.

[76] S. Elmore, Apoptosis: a review of programmed cell death, Toxicol. Pathol. 35 (2007) 495–516.

[77] K. Niizuma, H. Yoshioka, H. Chen, G.S. Kim, J.E. Jung, M. Katsu, N. Okami, Chan PH Mitochondrial and apoptotic neuronal death signaling pathways in cerebral ischemia, Biochim. Biophys. Acta 1802 (2010) 92–99.

[78] Q. Zhang, Y. Wu, P. Zhang, H. Sha, J. Jia, Y. Hu, Zhu J Exercise induces mitochondrial biogenesis after brain ischemia in rats, Neuroscience 205 (2012) 10–17.

[79] G.W. Dorn 2nd, R.B. Vega, D.P. Kelly, Mitochondrial biogenesis and dynamics in the developing and diseased heart, Genes Dev. 29 (2015) 1981–1991.

[80] M. Uittenbogaard, Chiaramello A Mitochondrial biogenesis: a therapeutic target for neurodevelopmental disorders and neurodegenerative diseases, Curr. Pharmaceut. Des. 20 (2014) 5574–5593.

[81] M.P. Murphy, Smith RA Targeting antioxidants to mitochondria by conjugation to lipophilic cations, Annu. Rev. Pharmacol. Toxicol. 47 (2007) 629–656.

[82] M. Dumont, K. Kipiani, F. Yu, E. Wille, M. Katz, N.Y. Calingasan, G.K. Gouras, M. T. Lin, Beal MF Coenzyme Q10 decreases amyloid pathology and improves behavior in a transgenic mouse model of Alzheimer's disease, J. Alzheimers Dis. 27 (2011) 211–223.

[83] B. Literati-Nagy, E. Kulcsar, Z. Literati-Nagy, B. Buday, E. Peterfai, T. Horvath, K. Tory, A. Kolonics, A. Fleming, J. Mandl, L. Koranyi, Improvement of insulin sensitivity by a novel drug, BGP-15, in insulin-resistant patients: a proof of concept randomized double-blind clinical trial, Horm. Metab. Res. 41 (2009) 374–380.

[84] H. Fujimoto, M. Higuchi, M. Koike, H. Ode, M. Pinak, J.K. Bunta, T. Nemoto, T. Sakudoh, N. Honda, H. Maekawa, K. Saito, K. Tsuchida, A possible overestimation of the effect of acetylation on lysine residues in KQ mutant analysis, J. Comput. Chem. 33 (2012) 239–246.

[85] H.Y. Cohen, S. Lavu, K.J. Bitterman, B. Hekking, T.A. Imahiyerobo, C. Miller, R. Frye, H. Ploegh, B.M. Kessler, Sinclair, DA Acetylation of the C terminus of Ku70 by CBP and PCAF controls Bax-mediated apoptosis, Mol. Cell 13 (2004) 627–638.

[86] C.X. Peng, J. Hu, D. Liu, X.P. Hong, Y.Y. Wu, L.Q. Zhu, J.Z. Wang, Disease-modified glycogen synthase kinase-3beta intervention by melatonin arrests the pathology and memory deficits in an Alzheimer's animal model, Neurobiol. Aging 34 (2013) 1555–1563.

[87] Z. Zhang, M. Song, X. Liu, S.S. Kang, I.S. Kwon, D.M. Duong, N.T. Seyfried, W. T. Hu, Z. Liu, J.Z. Wang, L. Cheng, Y.E. Sun, S.P. Yu, A.I. Levey, K. Ye, Cleavage of tau by asparagine endopeptidase mediates the neurofibrillary pathology in Alzheimer's disease, Nat. Med. 20 (2014) 1254–1262.

[88] Y. Yang, Z.H. Wang, S. Jin, D. Gao, N. Liu, S.P. Chen, S. Zhang, Q. Liu, E. Liu, X. Wang, X. Liang, P. Wei, X. Li, Y. Li, C. Yue, H.L. Li, Y.L. Wang, Q. Wang, D. Ke, Q. Xie, F. Xu, L. Wang, J.Z. Wang, Opposite monosynaptic scaling of BLP-vCA1 inputs governs hopefulness- and helplessness-modulated spatial learning and memory, Nat. Commun. 7 (2016), 11935.

[89] H.L. Li, H.H. Wang, S.J. Liu, Y.Q. Deng, Y.J. Zhang, Q. Tian, X.C. Wang, X.Q. Chen, Y. Yang, J.Y. Zhang, Q. Wang, H. Xu, F.F. Liao, J.Z. Wang, Phosphorylation of tau antagonizes apoptosis by stabilizing beta-catenin, a mechanism involved in Alzheimer's neurodegeneration, Proc. Natl. Acad. Sci. U. S. A. 104 (2007) 3591–3596.

[90] K. Foote, J. Reinhold, E.P.K. Yu, N.L. Figg, A. Finigan, M.P. Murphy, Bennett MR Restoring mitochondrial DNA copy number preserves mitochondrial function and delays vascular aging in mice, Aging Cell 17 (2018), e12773.

[91] Y.P. Zhang, X.M. Liu, J. Bai, X.J. Tian, X.C. Zhao, W. Liu, X.Y. Duan, W.N. Shang, H.Y. Fan, Tong C mitoguardin regulates mitochondrial fusion through MitoPLD and is required for neuronal homeostasis, Mol. Cell 61 (2016) 111–124.

[92] D. Meng, D. Yang, L. Hu, T. Liu, H. Zhang, X. Sun, X. Wang, Y. Chen, Y. Jin, R. Liu, Rifaximin protects against circadian rhythm disruption-induced cognitive impairment through preventing gut barrier damage and neuroinflammation, J. Neurochem. 163 (2022) 406–418.

[93] H. Kang, Sample size determination and power analysis using the G*Power software, J. Educ. Eval. Health Prof. 18 (2021) 17.